RAS isoform specific activities are disrupted by disease associated mutations during cell differentiation

Rohan Chippalkatti[1a], Bianca Parisi[1a], Farah Kouzi[1], Christina Laurini[1], Nesrine Ben Fredj[1] and Daniel Kwaku Abankwa[1*]

[1]Cancer cell biology and drug discovery group, Department of Life sciences and medicine, University of Luxembourg, 4362, Esch-sur-Alzette, Luxembourg

[a] these authors contributed equally

[*]correspondence: daniel.abankwa@uni.lu

Abstract

The Ras-MAPK pathway is aberrantly regulated in cancer and developmental diseases called RASopathies. While the impact of Ras on proliferation is typically assessed on various cancer cell lines, it is poorly established how Ras affects cellular differentiation.

Here we implement the C2C12 myoblast cell line to systematically study the effect of Ras mutants and Ras-pathway drugs on differentiation. We first provide evidence that the Pax7+ progenitors divide asymmetrically to replenish the major pool of transit amplifying cells that are ready to differentiate. Intriguingly, Ras isoforms have distinct roles in the differentiating culture, where K-Ras is more important than N-Ras to maintain the progenitor pool, and H-Ras is significant for the expansion of differentiated cells. While overexpression of wild-type K-Ras increases the fraction of differentiated cells at the expense of transit amplifying cells, all oncogenic mutants block further differentiation of transit amplifying cells. Interestingly, RASopathy associated mutants display distinct phenotypes. Notably variants that are also NF1-GAP resistant block differentiation as their oncogenic counterparts, albeit less. Profiling of targeted Ras-pathway drugs on oncogenic Ras mutants reveals their distinct abilities to restore normal differentiation as compared to triggering cell death. Interestingly, the MEK-inhibitor trametinib could broadly restore differentiation, while the mTORC1 inhibitor rapamycin broadly suppressed differentiation.

We expect that this quantitative assessment of the impact of Ras-pathway mutans and drug treatments on cellular differentiation will provide significant new insights into Ras biology and Ras-driven diseases.

Key words: Ras, cancer, RASopathy, C2C12, flow cytometry, inhibitors, differentiation

Introduction

Malignant tumors are characterized by abnormal proliferation and invasive growth of dedifferentiated tissue. The Ras-pathway is central to control cellular proliferation, differentiation and survival, and is dysregulated in virtually every cancer [1,2]. Three *RAS* genes, *KRAS*, *NRAS* and *HRAS,* are mutated in 19 % of human cancers making *RAS* the most frequently mutated oncogene [3]. Out of the two *KRAS* splice isoforms, K-Ras4A and K-Ras4B, the latter is the highest expressed isoform and the major focus of current drug development [4-6].

Ras membrane association is required for its activity. Membrane affinity is mediated by C-terminal lipid modifications of Ras by farnesyltransferase and palmitoyltransferases [7]. Farnesylation also mediates binding of Ras to trafficking chaperones, such as PDE6D and calmodulin, which facilitate its diffusion, followed by trapping on secretory organelles, and subsequent vesicular transport to the plasma membrane [8].

Canonical Ras signaling emerges at the plasma membrane, where extracellular mitogens activate receptor tyrosine kinases, such as epidermal growth factor receptor (EGFR), which indirectly relay the activation to guanine nucleotide exchange factors (GEFs), such as SOS. The active GTP-bound Ras then recruits effector proteins, such as Raf, PI3K and RalGDS from the cytosol to the membrane, leading to their activation [9]. Raf-kinases trigger the MAPK-pathway, which includes activation of downstream kinases MEK and ERK, the latter of which leads to well characterized changes that drive the cell cycle and thus proliferation [1]. The effector PI3K activates the kinase Akt, which further downstream turns on the mTORC1-pathway and thus cell growth and many other crucial cellular processes.

The active state of Ras is tightly regulated, with GTP-Ras becoming inactivated by GTPase-activating proteins (GAPs) [9]. The most prominently studied GAP is neurofibromin 1 (NF1), which is recruited to K-Ras nanodomains of the plasma membrane by one of three SPRED proteins [10-12]. Landmark structural data from the mid 1990s already explained how hotspot oncogenic mutations in codons 12,13 and 61 of Ras disable the GTP-hydrolysis of Ras by NF1 and other arginine-finger GAPs [13,14]. However, a GAP with a catalytic asparagine, the heterotrimeric G protein GAP RGS3, was recently shown to facilitate GTP-hydrolysis of all major oncogenic K-Ras mutants (G12D/V, G13C/D) [15], suggesting that a separated function of NF1 is disabled by oncogenic Ras.

In line with the mitogen-independent mutational activation of Ras, cancer cell assays typically assess the uncontrolled cell growth. Proliferation assays provided a wealth of data in cancer research, such as from large scale genetic and chemical screens [16-18]. However, among pathologists it is well established that dedifferentiation is the most unsettling hallmark of cancer [19]. Unfortunately, the functions of Ras during cellular differentiation are only poorly understood and typically not assayed.

This lack of understanding also impacts on the treatment development for another type of Ras-driven diseases. Germline mutations in the RAS-MAPK pathway lead to individually rare but collectively common developmental syndromes called RASopathies, which are characterized by facial malformations, short stature, cutaneous defects, cardiac hypertrophy and a pre-disposition to cancer [20,21]. They illustrate how even a mild overactivation of the MAPK-pathway during embryonal development perturb proper differentiation in multiple organ systems.

For instance, the RASopathy Noonan syndrome can be caused by the *KRAS-D153V* mutation, which in contrast to cancer associated hotspot mutations, is still sensitive to the GAP NF1, but shows increased effector binding [22]. Loss-of-function mutations in *NF1* itself lead to neurofibromatosis type I, one of the more common RASopathies [20]. This disorder shares some phenotypic similarities with the very rare RASopathy Legius syndrome, which is caused by heterozygous loss-of-function mutations in the *SPRED1* gene [23]. To analyze RASopathy mutants, dedicated low-throughput assays have been developed, which characterize early developmental defects during gastrulation or later in the whole organism in zebrafish and mouse animal models [24]. Yet, insufficient developmental or cell differentiation assay capacities may underlie the lack of efficacious therapies for most RASopathies [25].

These defects in RASopathies are consistent with the deep integration of MAPK-signaling already at the level of stem cell maintenance. During organismal development, pluripotent stem cells give rise to a vast variety of differentiated tissues [26]. Both during priming of naïve mouse embryonic stem cells and maintenance of pluripotency in human induced pluripotent stem cells is the MAPK-pathway involved [27,28]. In the fully developed organism, adult stem and progenitor cells are important for tissue homeostasis. In this function, they typically divide asymmetrically, giving rise to one stem-cell (referred to as self-renewal) and one committed or differentiated cell [26].

This fundamental homeostasis mechanism also appears to be maintained in the murine C2C12 myoblast cell line that was derived from a skeletal muscle of a 2-month old mouse. It is typically considered a more or less heterogenous population of myoblasts (myogenic progenitor cells), which proliferate symmetrically and remain undifferentiated under high serum conditions [29]. A small fraction of proliferating C2C12 cells expresses the muscle progenitor marker Pax7, a paired box transcription factor, as well as the basic helix-loop-helix transcription factors Myf5 [30]. Mitogen withdrawal in low serum culture conditions, rapidly triggers terminal differentiation of the majority of C2C12 cells into multinucleated myotubes within five days [29]. Differentiating cells downregulate Pax7 and upregulate myogenic factors, such as MyoD, myogenin and subsequently late differentiation markers, such as the motor protein myosin II heavy chain (MyHC) [31,32]. We recently described a flow cytometry-based assay protocol for the rapid analysis of C2C12 cell differentiation, which in contrast to current assays exactly quantifies the subpopulation of MyHC+ differentiated cells with and without genetic perturbations [33].

Interestingly, upon serum withdrawal a minor fraction remains undifferentiated and continues to express the progenitor marker Pax7, but no MyoD, Myf-5 or myogenin [30,32]. These features strikingly resemble quiescent satellite cells, the Pax7 positive adult stem cell population in muscles [34]. Currently, it is not fully resolved, how the minor fraction of myoblast progenitors is connected to a major fraction of differentiated cells. Myogenic differentiation is initiated by a rapid upregulation of SPRED1 upon serum switching and a subsequent decrease in MAPK-signaling [29,35]. In line with mitogens maintaining proliferation of myoblasts, oncogenic Ras prevents myogenic differentiation by downregulating the myogenic transcription factor MyoD and myogenin [36]. Conversely, overexpression of tumor suppressors, such as Sprouty2 and SPRED1 stimulate myogenesis even under high serum conditions [35,37]. Overall, the C2C12 cell model is one of the best characterized in vitro differentiation systems, which recapitulates essential in vivo processes [38].

The proper differentiation trajectories of tissues is perturbed in cancer and may lead to the emergence of rare cancer stem cells, which alone have the potential to seed new tumors, for example during metastization and relapse after therapy [26]. Current models suggest either reprogramming of differentiated cells or an evolution directly from stem/ progenitor niches [39,40]. Cancer stem cells are best characterized in functional and lineage tracing assays in vivo [41]. In vitro, flow cytometry can detect the expression of cancer stem cell markers, such as CD44+/CD24-, or identify cancer stem cells in the side population assay by their increased

drug efflux properties [42,43]. Low serum, non-adherent 3D spheroid cultures of human mammary stem/ progenitors cells, called mammospheres, were originally employed to maintain and study such cells in culture [44]. Subsequently these culture conditions were widely adopted to monitor cancer cell stemness from tumorospheres [45]. The simplicity of this assay enabled screening for compounds that may have a potential to target specifically cancer stem cells [46-48]. Current data suggest that *KRAS* is the strongest driver of stemness features, followed by *NRAS* and *HRAS* [49-51]. This potency order that was obtained across multiple model systems strikingly correlates with the *RAS* mutation frequency in cancer [52].

Salinomycin was one of the first cancer stem cell selective inhibitors that was described by the Weinberg group [53]. This and other compounds showed selective activity against K-Ras, but not H-Ras membrane organization, suggesting that K-Ras is of special significance in cancer stem cells [51,54,55]. While these natural products may become starting points for the development of more potent drugs, they contrast with inhibitors specifically raised against the target K-Ras. Two such inhibitors, sotorasib (AMG 510) and adagrasib (MRTX849) have recently been approved [56,57]. Essentially all of these covalent K-Ras-G12C specific inhibitors were built on the development of the compound ARS-1620 [58]. Moreover, MRTX849 derivatives gave rise to other non-covalent inhibitors, including MRTX1133 against K-Ras-G12D [59]. While allele specific inhibitors promise uniquely small side-effects, their limited applicability necessitates the development of more K-Ras inhibitors with new modes of action [60].

Here we utilized mainly flow cytometry to understand the impact of the three Ras isoforms, in particular of K-Ras4B, on C2C12 cell differentiation. We first provide a baseline to understand C2C12 cell differentiation, by elaborating that Pax7+ progenitors replenish a major pool of Pax7- transit amplifying cells, which give rise the MyHC+ differentiated cells. We then elaborate the distinct impact of Ras on differentiation using specific genetic perturbations. In addition, we demonstrate the applicability of our assay for medium throughput assessment of Ras-pathway drugs to restore differentiation that was perturbed by disease-associated Ras-isoforms and -alleles. Our assay is not only a novel tool to analyze Ras-mutants and -drugs, but provides an insight into how profoundly Ras-isoforms impact on differentiation.

STAR Methods

Key resources table

REAGENT or RESOURCE	SOURCE	IDENTIFIER
Antibodies		
Mouse monoclonal anti-Pax7 (Pax7); dilution 1:100 flow cytometry (FC)	Bio-Techne	Cat# MAB1675 RRID: AB_2159833
Mouse monoclonal anti-myogenin (5FD); dilution 1:100 FC; dilution 1:500 Western blotting (WB)	ThermoFisher Scientific	Cat# 14-5643-82 RRID: AB_1907431

Mouse monoclonal anti-Myosin 4 (MF20), eFluor 660; dilution 1:100 FC	ThermoFisher Scientific	Cat# 50-6503-82 RRID: AB_2574267
Mouse monoclonal anti-Myosin 4 (MF20); dilution 1:100 FC	ThermoFisher Scientific	Cat# 14-6503-82 RRID: AB_2572894
Mouse monoclonal anti-Pax7, Alexa Fluor 488 (Pax7); dilution 1:25 FC	Santa Cruz biotechnology	Cat# sc81648 RRID: AB_2159836
Mouse monoclonal anti-Histone H3 phospho (Ser10), Alexa fluor 647 (11D8); dilution 1:20 FC	BioLegend	Cat# 650805 RRID: AB_2564361
Mouse monoclonal anti-GAPDH, (GAPDH-71.1); dilution 1:10,000 WB	Merck	Cat# G8795 RRID: AB_1078991
Rabbit polyclonal anti-GAPDH; dilution 1:10,000 WB	Merck	Cat# G9545 RRID: AB_796208
Mouse monoclonal anti-Pax7 (Pax7); dilution 1:500 WB	Santa Cruz biotechnology	Cat# sc-81648 RRID: AB_2159836
Rabbit polyclonal anti-MYH1 (N-terminal); dilution 1:500 WB	Proteintech	Cat# 25182-1-AP RRID: AB_2879947
Rabbit polyclonal anti-p44/42 MAPK (Erk1/2); dilution 1:1000 WB	Cell Signaling	Cat# 9102 RRID: AB_330744
Mouse monoclonal anti-phopsho-p44/42 MAPK (Erk1/2) (Thr202/Tyr 204) (E10); dilution 1:2000 WB	Cell Signaling	Cat# 9106 RRID: AB_331768
Mouse monoclonal anti-Akt (pan) (40D4); dilution 1:2000 WB	Cell Signaling	Cat# 2920 RRID: AB_1147620
Rabbit monoclonal anti-phospho-Akt (Ser473) (D9E); dilution 1:1000 WB	Cell Signaling	Cat# 4060 RRID: AB_2315049
Mouse monoclonal anti-KRAS (3B10-F2); dilution 1:1000 WB	Merck	Cat# WH0003845M1 RRID: AB_1842235
Rabbit polyclonal anti-HRAS; dilution 1:1000 WB	Proteintech	Cat# 18295-1-AP RRID: AB_2121046
Mouse monoclonal anti-NRAS (F155); dilution 1:1000 WB (dilution 1:250 for si*HRAS*)	Santa Cruz biotechnology	Cat# sc-31 RRID: AB_628041
IRDye 680RD goat anti-Rabbit IgG; dilution 1:10,000 WB	LI-COR Biosciences	Cat# 926-68071 RRID: AB_10956166
IRDye 680LT donkey anti-Mouse IgG; dilution 1:10,000 WB	LI-COR Biosciences	Cat# 926-68022 RRID: AB_10715072
IRDye 800CW goat anti-Rabbit IgG; dilution 1:10,000 WB	LI-COR Biosciences	Cat# 926-32211 RRID: AB_621843
IRDye 800CW donkey anti-Mouse IgG; dilution 1:10,000 WB	LI-COR Biosciences	Cat# 926-32212 RRID: AB_621847
Bacterial and virus strains		
E. coli DH10B	New England BioLabs	Cat# C3019I
Biological samples		

N/A	N/A	N/A
Chemicals, peptides, and recombinant proteins		
Sotorasib (AMG 510)	MedChem Express	Cat# HY-114277 CAS# 2296729-00-3
ARS-1620	MedChem Express	Cat# HY-U00418 CAS# 1698055-85-4
MRTX1257	MedChem Express	Cat# HY-114436 CAS# 2206736-04-9
MRTX1133	MedChem Express	Cat# HY-134813 CAS# 2621928-55-8
Trametinib	MedChem Express	Cat# HY-10999 CAS# 871700-17-3
Adagrasib (MRTX849)	Selleckchem	Cat# S8884 CAS# 2326521-71-3
Cysmethynil	Cayman Chemical	Cat# 14745 CAS# 851636-83-4
Rapamycin	BioVision	Cat# 1568 CAS# 53123-88-9
Tipifarnib	Selleckchem	Cat# S1453 CAS# 192185-72-1
BI-3406	MedChem Express	Cat# HY-125817 CAS# 2230836-55-0
Gefitinib	Biorbyt	Cat# orb545838 CAS# 184475-35-2
Dimethyl sulfoxide (DMSO)	PanReac AppliChem	Cat# A3672 CAS# 67-68-5
Critical commercial assays		
Gateway LR Clonase II enzyme mix	ThermoFisher Scientific	Cat# 11791020
APC conjugation kit – Lightning-Link	Abcam	Cat# ab201807
PE/R-Phycoerythrin conjugation kit – Lightning Link	Abcam	Cat# ab102918
Cell proliferation staining reagent – Deep Red Fluorescence (Cytopainter deep red)	Abcam	Cat# ab176736
Cell proliferation staining reagent – Orange Fluorescence (Cytopainter orange)	Abcam	Cat# ab176737
Bio-Rad Protein Assay Kit I	Bio-Rad	Cat# 5000001
Pierce Protease Inhibitor Tablets	ThermoFisher Scientific	Cat# A32963
PhosSTOP	Merck	Cat# 4906845001
Lipofectamine RNAiMAX Transfection Reagent	ThermoFisher Scientific	Cat# 13778075
Lipofectamine 2000 Transfection Reagent	ThermoFisher Scientific	Cat# 11668019
TRIzol Reagent	ThermoFisher Scientific	Cat# 15596018
SuperScriptIII Reverse Transcriptase	ThermoFisher Scientific	Cat# 18080093
SsoAdvanced Universal SYBR Green Supermix	Bio-Rad	Cat# 1725274
FITC Annexin V Apoptosis detection kit I	BD Biosciences	Cat# 556547
Experimental models: Cell lines		
Mouse cell line, C2C12	ATCC	Cat# CRL-1772 RRID: CVCL_6974
Experimental models: Organisms/strains		
N/A	N/A	N/A

Oligonucleotides		
Custom qPCR primer: KRAS human_F 5'-3' sequence TACAGTGCAATGAGGGACCA	Genecust	N/A
Custom qPCR primer: KRAS human_R 5'-3' sequence TCCTGAGCCTGTTTTGTGTCT	Genecust	N/A
Custom qPCR primer: NRAS mouse_F 5'-3'sequence TAACCTCTACAGGGAGCAAAT	ThermoFisher Scientific	N/A
Custom qPCR primer: NRAS mouse_R 5'-3' sequence GTTGACACAAAGCAAGCCCAC	ThermoFisher Scientific	N/A
Custom qPCR primer: HRAS mouse_F 5'-3' sequence AGCAGATCAAGCGGGTGAAA	ThermoFisher Scientific	N/A
Custom qPCR primer: HRAS mouse_R 5'-3' sequence ATCGGGTGGGTTCAGTTTCC	ThermoFisher Scientific	N/A
Custom qPCR primer: GAPDH mouse_F 5'-3' sequence TGGTGAAGGTCGGTGTGAA	Eurogentec	N/A
Custom qPCR primer: GAPDH mouse_R 5'-3' sequence ATGAAGGGGTCGTTGATGG	Eurogentec	N/A
Negative control siRNA	QIAGEN	Cat# 1027310 GeneGlobe ID: SI03650325
Human *HRAS* siRNA (FlexiTube siRNA) 5'-3'sequence CGGAAGCAGGUGGUCAUUA	QIAGEN	Cat# 1027417 GeneGlobe ID: SI02654806
Mouse *KRAS* siRNA (targeting both *KRAS*4A and 4B transcripts) (ON-TARGETplus SMARTpool siRNA) 5'-3' sequences GAACAGUAGACACGAAAA AGCAAGGAGUUACGGGAUU GGUUGGAGCUGGUGGCGUA GGUGUACAGUUAUGUGAAU	Horizon Discovery	Cat# L-043846-01-0005
Custom siRNA: Mouse *NRAS* siRNA 5'-3' sequence GCAAAUUAAGCGUGUGAAAUUU	Horizon Discovery	N/A
Recombinant DNA		
C453-E04: attB4-CMV51p>-attB5	FNL Combinatorial Cloning Platform, RAS-Initiative	Addgene# 162973
pDest-305 (attR4-attR2)	FNL Combinatorial Cloning Platform, RAS-Initiative	Addgene# 161895

C512-E01: attB5r-mEGFP-nostop-attB1r	FNL Combinatorial Cloning Platform, RAS-Initiative	Addgene# 162940
Hs. KRAS4b-WT	RAS mutant collection V2.0, RAS-Initiative	Addgene# 83129
Hs. KRAS4b-G12C	RAS mutant collection V2.0, RAS-Initiative	Addgene# 83130
Hs. KRAS4b-G13D	RAS mutant collection V2.0, RAS-Initiative	Addgene# 83133
Hs. KRAS4b-Q61H	RAS mutant collection V2.0, RAS-Initiative	Addgene# 83140
pDest305-CMV-mEGFP-K-Ras4B WT	This paper	N/A
pDest305-CMV-mEGFP-K-Ras4B G12C	This paper	
pDest305-CMV-mEGFP-K-Ras4B G13D	This paper	
pDest305-CMV-mEGFP-K-Ras4B Q61H	This paper	
pmEGFP-KRas4B-G12V	[61]	N/A
pmEGFP-HRas-G12V	[61]	N/A
pmEGFP-HA-NRas-G12V	[61]	N/A
pEGFP-KRAS4B-G12D	[62]	N/A
pmGFP-KRas4B-G12V-S17N	This paper	N/A
pEYFP-wt KRas	[22]	N/A
pEYFP-KRAS4b-T58I	[22]	N/A
pEYFP-KRAS4b-D153V	[22]	N/A
pEYFP-KRAS4b-V14I	[22]	N/A
pEYFP-KRAS4b-P34R	[22]	N/A
pEYFP-KRAS4b-P34L	[22]	N/A
pEYFP-KRAS4b-K5N	[22]	N/A
pEYFP-KRAS4b-K5E	[22]	N/A
pEYFP-KRAS4b-Q22E	[22]	N/A
pEYFP-KRAS4b-G60R	[22]	N/A
pEYFP-KRAS4b-Y71H	[63]	N/A
Software and algorithms		
GuavaSoft version4.0	Cytek Biosciences	N/A
Leica Application Suite X version 4.12	Leica Microsystems	RRID: SCR_013673
GraphPad Prism version 9.5.1	GraphPad	RRID: SCR_002798
Fiji version 2.9.0	Schindelin, 2012	RRID: SCR_002285
FlowFate version 1.2	[33]	N/A
Image Studio software version 5.2	LI-COR Biosciences	N/A
Bio-Rad CFX Manager (version 3.1)	Bio-Rad	N/A
Other		
Guava easyCyte 6HT 2L flow cytometer	Cytek Biosciences	Cat# 0500-4007
Odyssey CLx Infrared Imaging System	LI-COR Biosciences	Cat# LI9140-00
CFX-connect real-time PCR Detection System	Bio-Rad	Cat# 1855200
Dulbecco's Modified Eagle's Medium (DMEM)	ThermoFisher Scientific	Cat# 11965092
Fetal bovine serum (FBS)	ThermoFisher Scientific	Cat# 10270106
Horse serum (HS)	ThermoFisher Scientific	Cat# 16050130

L-glutamine (200 mM)	ThermoFisher Scientific	Cat# A2916801
Penicillin-Streptomycin (10,000 U/mL)	ThermoFisher Scientific	Cat# 10378016
Opti-MEM Reduced Serum Medium	ThermoFisher Scientific	Cat# 31985070
Hank's balanced salt solution (HBSS)	Lonza	Cat# BE10-547F
Paraformaldehyde 16 % (w/v)	Avantor	Cat# 30525-89-4
TWEEN 20	Merck	Cat# P9416
Triton X-100	Merck	Cat# T8787
BsrGI-HF (20,000 U/mL)	New England BioLabs	Cat# R3575S

Cell Culture and transfections

C2C12 cells were maintained in Dulbecco's modified Eagle Medium (DMEM) supplemented with ~9 % (v/v) fetal bovine serum (FBS), 2 mM L-glutamine and 1 % penicillin/streptomycin (high serum culture medium). Cells were incubated in a humidified incubator at 37 °C, with 5 % CO_2 and passaged when reaching 50 – 60 % confluency. Passage numbers beyond ten were not employed. Cell culture medium was exchanged with DMEM supplemented with ~2 % horse serum (HS), 2 mM L-glutamine and 1 % penicillin/streptomycin (low serum culture medium) to induce differentiation at 90 % confluency. For experiments lasting three to five days fresh DMEM + 2% HS was added every day.

Preparation of expression constructs

Plasmid constructs used for transfection were generated by multisite gateway cloning [64]. To generate the final expression constructs, LR Clonase II enzyme mix was used to perform recombination of the entry clones encoding the promoter, the fluorescent tag and the gene of interest with the pDest-305 destination vector. The reaction mix was transformed into ccdB-sensitive *E.coli* strain DH10B. Colonies resistant to ampicillin were selected for screening of their plasmid DNA by restriction digestion with BsrGI-HF enzyme. Plasmids with the expected fragment sizes were then further validated with sequencing.

Plasmid DNA transfection

C2C12 cells were seeded in high serum medium at a density of 100,000 cells per mL of a 6-well plate (#10062-892, Avantor) and transfection was performed after the cells reached 50 – 60 % confluency (typically 24 h after seeding). Transfection was performed according to the protocols provided by the manufacturer. 2 µg of plasmid DNA and 7.5 µL Lipofectamine 2000 were added to 250 µL Opti-MEM medium. The mixture was vortexed, incubated at 22 - 25 °C for 10 min and subsequently added dropwise to one well of a 6-well plate. Medium was exchanged with fresh high serum medium after 4 h. After further 24 h incubation with high serum, medium was exchanged with low serum medium to induce differentiation.

Knockdown by siRNA transfection

Any siRNAs were transfected using Lipofectamine RNAiMAX diluted in Opti-MEM medium. Typically, 100 nM of each siRNA and 7.5 µL of Lipofectamine was added to 250 µL of Opti-MEM medium, mixed

and incubated at 22 – 25 °C for 10 min. Cells were transfected at 50 – 60 % confluency by adding this mixture. After 24 h of incubation with the siRNA-Lipofectamine mixture, the medium was substituted with fresh high serum medium. After 3 – 4 h, high serum medium was exchanged with low serum medium, and cells were cultured in low serum medium that was replaced every day.

Antibody conjugation with Allophycocyanin (APC) or Phycoerythrin (PE)

For flow cytometry experiments anti-Pax7 and anti-myogenin antibodies were conjugated to APC with the reagents provided in the APC conjugation kit – Lightning link. Anti-Myosin 4 Monoclonal antibody (anti-MyHC) was conjugated with PE with the components provided in the PE/R-Phycoerythrin conjugation kit – Lightning link kit. The modifier reagent and quencher reagent were contained in both kits. Additionally, the APC conjugation reaction mix was supplied with the APC kit and the PE conjugation reaction mix was supplied with the PE/R-Phycoerythrin kit. Anti-Pax7 or anti-myogenin antibodies at a concentration of 1 mg/ mL and 100 µL volume were mixed with 100 µg APC Conjugation Reaction Mix, together with 10 µL of Modifier Reagent. Similarly, 100 µL of 0.5 mg/mL anti-MyHC antibody was mixed with 100 µg PE Conjugation Reaction Mix with 10 µL of Modifier Reagent. This mixture was stored in the dark at 22 – 25 °C for 3 – 4 h. Subsequently, the conjugation reaction was stopped by adding 10 µL quencher reagent to the conjugation mix. The conjugated antibody solution was used at a dilution of 1:100 and stored at 4 °C for up to 6 months.

The degree of labelling (DOL) was calculated according to the formula, DOL = (Amax × MW × dilution factor)/(ε × [conjugate]). MW is the molecular weight of IgG (~150,000 g/mol), and ε is the molar extinction coefficient of the dye (for e.g. 700,000 M^{-1} cm^{-1} for APC), [conjugate] = {[A280 – (Amax × Cf)]/1.4} × dilution factor. Here, [conjugate] is the concentration in mg/ mL of the antibody conjugate, 'dilution factor' is the fold of dilution used for spectral measurements. A280 is the absorbance of the conjugate at 280 nm and Amax is the absorption maximum of APC. Cf is the absorbance correction factor and the value 1.4 is the extinction coefficient of IgG in mg/mL. For APC, Cf is 0.22. We obtained 0.5 – 1 moles of APC per antibody, which falls within the optimal range for labelling. Similar results were obtained with the PE conjugation kit.

Flow cytometry

Cells were seeded at a concentration of 100,000 cells/mL per well of a 6 well plate. This was followed by transfection with the required plasmids or siRNAs and a low serum culture period for the time indicated in the figures or figure legends. Fresh low serum, where required with drug/ compound, was added every day. Cells were then harvested by trypsinization with 0.05 % (w/v) trypsin EDTA (1×) for 5 min and pelleted by centrifugation at 500 × g for 5 min. The subsequent steps were performed at 22 - 25 °C. The cell pellet was subsequently fixed with 4 % (w/v) formaldehyde in PBS for 10 min. After washing with PBS, cells

were permeabilized with 0.5 % (v/v) Triton X-100 in PBS for 10 min. Subsequently cells were washed with 0.05 % (v/v) Tween 20 in PBS (PBST) and immunolabelled with fluorescent-dye conjugated primary antibodies at the indicated dilutions in PBST for 1 h at 4 °C. Subsequently cells were pelleted by centrifugation at 500 × g for 5 min and resuspended in PBST for flow cytometric analysis.

We first gated around 30,000 cells based on their forward and side scatter properties to exclude debris or dead cells. The intact cells thus obtained were further analyzed for expression markers using dot plots. In general, for transfected samples the intact cell fraction contained EGFP-variant construct expressing cells ranging from 2,000 to 10,000, depending on the day of collection and treatment condition. EGFP-variants and Alexa Fluor 488 were excited with the 50 mW photodiode 488 nm laser and the fluorescent signal was detected using the Green-B filter (band pass 525/30 nm) on a Guava Luminex easyCyte 6HT 2L flow cytometer. APC or eFluor 660 were excited using 100 mW photodiode 642 nm laser and detected using the Red-R filter (band pass 661/15 nm). PE was excited using 50 mW photodiode 488 nm laser and detected using the Yel-B filter (band pass 583/26 nm). An unlabeled control sample was always included as a control to correct for autofluorescence and spectral overlap in case of PE. EGFP was corrected via digital compensation using single color control samples.

Labelled or EGFP-variant expressing cells were quantified using the 'Quad Stat plot' feature on the GuavaSoft 4.0 software. The laser power and the voltage gain settings were adjusted such that the unlabeled events appeared below the level of 10^1 relative fluorescence units (RFU). Two EGFP-expression windows were defined, 'GFP-low' with 10^1 and 10^2 RFU and 'GFP-high' with 10^2 and 10^5 RFU. This allowed to quantitate differentiation in dependence of the EGFP-expression level. The majority of data were analyzed in the GFP-low window, which produced a phenotype comparable to non-transfected C2C12 cells. A detailed step-by-step procedure of sample preparation, data acquisition and analysis is described in our previous work [33].

To evaluate drug induced cell toxicity, gating was applied based on forward and side scatter characteristics to separate total events into intact cells and debris. The percentage of intact cells among the total events was then plotted for each EGFP-construct and drug treatment to estimate cell toxicity.

Cell proliferation analysis in dye dilution experiments

A 500 × stock solution of Cytopainter deep red/Cytopainter orange was prepared as described by the manufacturer and stored at -20°C. A 1 × working solution was prepared on the day of labelling in Hank's balanced salt solution (HBSS). Cells from a confluent flask were detached with trypsinization, pelleted by centrifugation at 200 × *g* for 3 min and 1 mL high serum medium was added to the pellet. Cells were then counted on a Z1 particle counter (Beckman Coulter) to obtain 100,000 cells per 1 mL high serum medium. Cells were again pelleted by centrifugation at 500 × *g* for 5 min, resuspended in 500 µL cytopainter working solution and incubated in the dark at 37 °C for 15 min. Cells were once more pelleted (500 × *g* for 5 min)

and the pellet was washed once with 500 μL HBSS. After another round of pelleting, cells were finally resuspended with 1 mL high serum medium. 200 μL from this cell suspension was kept aside as the day 0 followed by fixation with 4 % (w/v) PFA. Out of the remaining 800 μL, 200 μL cell suspension containing 20,000 cells was dispensed per well in 3 wells of a 6-well plate containing 2 mL high serum medium. Cells were then incubated for 3 days in the cell culture incubator. Cells from one well were collected by trypsinization on day 1, day 2 and day 3 and processed for immunofluorescence with mouse monoclonal anti-Pax7, Alexa Fluor 488 antibody. Cytopainter deep red fluorescence was detected by 642 nm laser excitation and using the Red-R emission filter (band pass 661/15 nm). Half-life ($t_{1/2}$) of cytopainter decay was calculated using the one-phase decay equation in Prism 9.0, $Y = (Y0 - plateau) \times \exp(-K \times X) + plateau$, with $t_{1/2} = \ln(2)/K$. Here, X is time (days), Y is the cytopainter mean fluorescence intensity, Y0 is the Y value at day 0 which decays with one phase to plateau and K is the rate constant expressed as a reciprocal of the X axis unit.

The 'Misc parameters' feature on the GuavaSoft software provides the number of events per microliter of each sample, which allowed us to calculate the cell concentration per mL of Pax7+ and Pax7- fractions.

To analyze cell proliferation in cells transfected with mEGFP tagged wt K-Ras and K-RasG12V constructs, 100,000 cells/ mL were first seeded in all wells of a 6 well plate. Each construct was transfected in all wells of a 6 well plate. Transfected cells were then harvested by trypsinization, cells from all wells were pooled in a single 15 ml falcon tube and cell concentration was determined with a Z1 particle counter. Cell staining with cytopainter orange reagent was then carried out in exactly as described above for cytopainter deep red. Cells labelled with cytopainter orange were then fixed and immunolabelled with APC conjugated anti-Pax7 antibody. Cytopainter orange fluorescence was detected with 488 nm laser excitation and the Yel-B emission filter (band pass 583/26 nm). Cytopainter orange fluorescence signal for Pax7+ and Pax7- fractions was measured specifically for cells in the 'GFP-low' window.

Cell toxicity analysis with 7-AAD

The cell impermeable dye 7-Aminoactinomycin D (7-AAD) is excluded from intact cells but intercalates into the genomic DNA of late apoptotic and necrotic cells since the plasma membrane integrity of these cells is compromised. The toxicity of K-RasG12C inhibitors was analyzed in cell fractions transfected with pDest305-CMV-mEGFP-K-RasG12C. Cells were treated 24 h after transfection with DMSO, sotorasib (AMG 510), MTRX1257 and adagrasib (MTRX849) in low serum for three days at indicated concentrations. The medium was first aspirated from drug treated cells to collect the 'supernatant' fraction of dead cells. The 'adherent' fraction of cells was collected by trypsinization. After centrifugation at 500 × *g* for 5 min and a washing step with PBS, both fractions were labelled with the provided 7-AAD solution for 15 min on ice according to the manufacturer instructions. The 7-AAD fluorescence was detected using a 100 mW photodiode 642 nm laser the Red-B filter (band pass 635/40 nm) by flow cytometry. Cells expressing GFP-constructs and labelled with 7-AAD were gated and counted using the Quad Stat plot

feature on GuavaSoft software. Cell count of GFP+ and 7AAD+ cells was normalized to the total cell count and plotted for each drug treatment.

Microscopy

Brightfield images were acquired with a 20 × objective of a Leica DMI3000 B inverted microscope equipped with a Leica DFC360 FX digital camera. Samples were illuminated using pE400max LED white light source from CoolLED. Images were analyzed with Leica LAS X software.

Immunoblotting

Cells were seeded at a density of 100,000 cells/ mL in each well of a 6-well plate, transfected and then cultured in low serum as indicated in the figures. Cells were then washed with ice-cold PBS and lysed for 30 min on ice using a total of 100 µL of lysis buffer (10 mM Tris pH 7.5, 150 mM NaCl, 0.5 mM EDTA, 0.2% NP40) supplemented with one tablet of protease inhibitor cocktail per 10 mL lysis buffer. The lysis buffer was additionally supplemented with one tablet per 10 mL of the PhosSTOP phosphatase inhibitor cocktail. Cells were collected using a scraper and incubated on ice for 30 min with intermittent vortexing. Lysates were cleared by centrifugation at 13,000 × *g* for 10 min at 4 °C. Supernatants were collected and quantified by the Bradford assay using Bio-Rad Protein Assay Kit, followed by heating at 95 °C for 5 min. Protein samples were then resolved on denaturing SDS-PAGE. A 6 % resolving gel was used for detection of MyHC, 10 % resolving gel for Pax7, p44/42 Erk1/2, Akt and 15 % resolving gel for detection of myogenin, K-Ras (total K-Ras, both 4A and 4B isoforms), H-Ras, N-Ras. Subsequently, separated proteins were transferred onto a nitrocellulose blotting membrane 0.2 µm by using a TransBlot turbo Transfer System (Bio-Rad). The blots were probed as indicated in the figures with the antibodies diluted as described in the Key Resources Table. The membranes were washed 3 times with PBST and then incubated with anti-mouse or anti-rabbit IRDye800CW or IRDye680RD/LT conjugated secondary antibodies. Finally, protein bands were detected using a LI-COR ODYSSEY CLx system. Band intensities for each protein per condition were quantified using Fiji and normalized to GAPDH. The relative abundance of phosphorylated p44/42 ERK 1/2 and phospho-Akt was quantified by obtaining a ratio of the intensities for the phosphorylated proteins with respect to the total protein.

Quantitative RT-PCR of gene transcripts

Cells were seeded at a density of 100,000 cells/ mL of a 6-well plate and transfected with siRNAs directed against *KRAS*, *NRAS* and *HRAS*. Note that the *HRAS* siRNA against the human mRNA was also targeting the identical sequence of the mouse mRNA. After culturing in low serum medium, cells were collected as indicated in the figures. Total RNA was isolated using Trizol according to the manufacturer's protocol. Reverse transcription was performed with 1 µg of total RNA using SuperScriptIII Reverse Transcriptase. The relative abundance of *KRAS*, *NRAS* and *HRAS*, gene transcripts was analyzed by using SsoAdvanced

Universal SYBR Green Supermix on the CFX-connect real-time PCR instrument (Bio-Rad) and Bio-Rad CFX Manager Software. Specific amplicons were detected for *KRAS* (both K-Ras4A and K-Ras4B splice variants), *NRAS HRAS*, and *GAPDH*. Forward and reverse primer sequences *KRAS* and *NRAS* amplicons were described previously [5,65]. Primers for amplification of *HRAS* and *GAPDH* were designed using the online tool 'OligoPerfect Primer Designer'. The mRNA sequences of mouse *HRAS* (NM_008284.3) and *GAPDH* (NM_008084.4) were used as templates for primer design. The relative mRNA expression level was calculated using the $2^{-\Delta\Delta Ct}$ method by normalizing to *GAPDH* expression [66].

Data and Statistical analysis

Prism 9 (GraphPad) was used for the preparation of plots, heatmaps, data and statistical analysis. The number n of analyzed cells that was employed for statistical calculations was at least 2000. These originated from N independent biological repeats as indicated in the figure legends. Bar plots show mean ± SD, if not stated otherwise. Statistical analysis of flow cytometry data was performed by employing the Fisher's Exact test, unless otherwise mentioned in the legends. Immunoblotting data were compared using the One-way ANOVA. Half-lives and slopes were compared using the Mann-Whitney test.

A p-value < 0.05 is considered statistically significant, and the statistical significance levels are annotated as follows: * $p < 0.05$; ** $p < 0.01$; *** $p < 0.001$; **** $p < 0.0001$.

Results

Benchmarking of flow cytometry-based analysis of C2C12 differentiation

Differentiation stage-specific markers of mouse muscle C2C12 cells correlate with those identified during muscle development *in vivo* (***Figure 1A***) [38]. Both MAPK- and PI3K-pathway are characteristically regulated during differentiation [29,35,67]. The C2C12 model therefore offers the opportunity to study the impact of Ras-pathway disease variants and targeted drug treatments on cellular differentiation.

We first benchmarked this assay against conventional phenotypic and immunoblotting-based differentiation analysis. C2C12 cell myoblasts assume a roundish-rhomboid morphology when cultured in high serum (day 0) (***Figure 1B***). Medium switching to low serum induces differentiation, which alters the morphology of cells to become increasingly more spindle shaped. From day 2 to day 3 after serum switching the number of spindle shaped cells visibly increased, and further elongation with subsequent fusion resulted in a robust myotube assembly at day 5 (***Figure 1B***). While determining the fraction of nuclei incorporated into myotubes can measure the overall progression of differentiation as the fusion index, this and related methods are quite tedious and allow only for the analysis of small cell numbers [68].

In addition, muscle progenitor and differentiation markers are commonly analyzed using immunoblotting, which however captures only the averaged response across the heterogenous, differentiating cell pool. This

became obvious when we compared immunoblotting- and flow cytometry-derived results of various muscle differentiation markers during the 5-day differentiation period. Immunoblotting revealed a nearly constant Pax7 protein expression levels (***Figure 1C***), which was matched by an almost constant fraction of Pax7 positive (Pax7+) cells that exhibited a constant mean Pax7 intensity in the flow cytometry-based analysis (***Figure 1D***). By contrast, analysis of the early differentiation marker myogenin by immunoblotting suggested a linear increase of the muscle-specific transcription factor during differentiation (***Figure 1E***). This increase is however not due to an increased number of myogenin positive cells, but an increased mean expression level of the transcription factor in the population, as revealed by the flow cytometry data (***Figure 1F***). Both immunoblotting (***Figure 1G***) and flow cytometric analysis (***Figure 1H***) confirmed that the expression of the late differentiation marker myosin heavy chain (MyHC) rapidly increased from day 3 onward. In this case both the fraction of MyHC+ cells and the mean expression level in the population increased (***Figure 1H***). The flow cytometry-based analysis of C2C12 cell differentiation therefore resolves population level differences in the expression of differentiation markers that may remain hidden in other common types of differentiation analyses. We therefore recently established a protocol to quantify C2C12 cell differentiation using the flow cytometric quantification of the MyHC+ fraction, which we furthermore automated by our custom R-script software FlowFate [33].

The sensitivity of this assay furthermore enabled us to detect a decline in differentiation potential with an increase in passage number. Cells with the passage number six (***Figure 1G,H***) arrived at ~20 % MyHC+ cells at day 3, while this fraction declined to ~15 % in passage eight and slightly further to ~14 % in passage ten (***Figure1 – figure supplement 1 A-D***). At the same time, the number of differentiated cells at day 0 in high serum increased in the same order, suggesting that a leakage into differentiation occurs due to passaging even in high serum. As this reduced the net change of the fraction of differentiated cells, i.e. the dynamic range of this assay, we aimed at employing cells with passage numbers from six to nine and included internal references wherever possible. Nevertheless, a residual background fluctuation inherent to variations caused by the passage numbers can be observed in our data that were composed from independent biological repeats across a longer time span.

Differentiated cells arise from the major pool of Pax7-/ MyHC- transit amplifying cells

Our analysis revealed that the muscle progenitor marker Pax7 is expressed by a minor sub-population of C2C12 cells (< 1%) before and after induction of differentiation (***Figure 2A***). It is therefore unlikely that this population of myoblasts provides the bulk of differentiated Pax7-/ MyHC+ myotubes. Instead, double labelling revealed that concomitant with the increase of the Pax7-/ MyHC+ differentiated cells, a Pax7-/MyHC- subpopulation decreased that constitutes the bulk of the C2C12 cell line (***Figure 2A***). This strongly suggests that the MyHC+ differentiated cells arise from the Pax7-/ MyHC- cells.

To understand how this large pool of Pax7-/ MyHC- cells is maintained under high serum conditions, we analyzed the proliferation of the Pax7+ and Pax7- populations by co-labelling Ser10-phosphorylated

histone H3 (pH3), a marker of mitotic and proliferative activity [69]. While ~22 % of Pax7+ myoblasts were also pH3+ at day 0 in high serum, only ~5 % of Pax7- cells were pH3+, suggesting that these latter cells have a low mitotic activity. After switching to low serum, the fraction of mitotically active Pax7+ cells dropped to ~12 % (***Figure 2B***), while the Pax7- population almost stopped dividing (***Figure 2C***).

The higher proliferation rate of Pax7+ cells in high serum was further supported by dye-dilution experiments. The non-toxic cytopainter dye is diluted ~2-fold during each cell division, which was reflected by the decrease in the geometric means of fluorescence intensities in an exponentially growing cell population (***Figure 2D***). When cultured under high serum, the cytopainter labelling decayed at a comparable rate in both Pax7+ and Pax7- subpopulations (***Figure 2E***). At the same time, the number of Pax7- cells increased exponentially during the 3-day culture in high serum, while that of Pax7+ cells only marginally increased (***Figure 2F***).

This proliferation pattern is reminiscent of other developmental systems where a minor pool of progenitors asymmetrically divides to generate one progenitor and one transit amplifying cell. The latter then expand exponentially, while the progenitor pool is preserved [70]. This setup is not only critical during development but also for tissue homeostasis and regeneration in the adult.

Our data therefore suggest that under high serum conditions, the Pax7-/ MyHC- transit amplifying cells are replenished via asymmetric cell divisions by the highly proliferative Pax7+/ MyHC- progenitors, which explains the similar half-life of Pax7+ and Pax7- cell dye dilutions (***Figure 2E***). Upon serum switching, the Pax7-/ MyHC- cells divide slowly and symmetrically. It furthermore continues to be replenished by the asymmetrically dividing progenitors, which explains the exponential expansion of Pax7- cells. With terminal differentiation, the Pax7- pool becomes post-mitotic and gradually forms myocytes and myotubes while expressing MyHC (***Figure 2G***).

K-Ras4A/B are needed for progenitor maintenance while H-Ras promotes differentiation

It was previously suggested that the three cancer associated Ras genes, *KRAS*, *NRAS* and *HRAS* all promote muscle differentiation via the PI3K- pathway. However, the individual contributions of the Ras genes on the above established three subpopulations of C2C12 cells is unknown. We therefore utilized siRNA-mediated knockdown to specifically downmodulate endogenous *RAS* isoforms and analyzed the effect on the Pax+/ MyHC- progenitors, Pax7-/ MyHC- transit amplifying cells and Pax7-/ MyHC+ terminally differentiated cells during differentiation.

Ras isoform specificity of knockdowns was validated by both immunoblotting (***Figure 3-figure supplement 1***) and quantitative RT-PCR (***Figure 3-figure supplement 2***). This analysis surprisingly revealed that knockdown of *NRAS* significantly increased K-Ras and to some extent H-Ras protein expression levels on day 1 (***Figure 3-figure supplement 1F***), which was for K-Ras also reflected on the mRNA-level (***Figure 3-figure supplement 2D***). In addition, *NRAS* knockdown also downmodulated H-Ras mRNA on day 4 (***Figure 3-figure supplement 2D***). Otherwise, all knockdowns remained isoform specific

with an average knockdown efficiency of ≥ 50 % on the protein level during the 5-day differentiation period (***Figure 3-figure supplement 1C,E,G***).

Specific knockdown of *KRAS* (i.e., of both K-Ras4A and K-Ras4B proteins) led to a significant reduction of progenitors that is more clearly visible from day 3 onwards (***Figure 3A***). Consequently, a slight but not significant drop in the fraction of transit amplifying cells was noticeable (***Figure 3B***). Importantly, from day 3 on the population of differentiated cells was significantly increased upon *KRAS* knockdown (***Figure 3C***). A similar, albeit attenuated effect notably in the population of differentiated cells was observed with the *NRAS* knockdown (***Figure 3D-F***). It is plausible to assume that the smaller effect is due to the *NRAS* knockdown induced upregulation of K-Ras and H-Ras. A markedly different outcome was observed upon knockdown of *HRAS*, which did not alter the progenitor fraction (***Figure 3G***) but slightly increased the fraction of transit amplifying cells (***Figure 3H***), which then resulted in a significantly decreased fraction of differentiated cells notably from day 3 onward (***Figure 3I***).

Our observations are incompatible with the alternative concept that the total Ras-level determines differentiation. Instead, specific knockdown of *RAS* isoforms reveals their distinct impact on C2C12 cell subpopulations during differentiation.

K-Ras4A/B sustain MAPK-signaling, while H-Ras sustains both MAPK- and PI3K-signalling during differentiation

Induction of differentiation is accompanied by a characteristic drop in MAPK-activity, while signaling through the PI3K-pathway promotes myogenesis and terminal differentiation of C2C12 cells [29,35,67].

To understand which Ras isoform is activating these two major pathways during differentiation, we analyzed samples with individual knockdowns of *KRAS*, *NRAS* or *HRAS* by immunoblotting for phosphorylated ERK 1/2 (pERK) and phosphorylated Akt1 (pAkt), respectively. We observed a substantial decrease of relative pERK levels upon *KRAS* and *HRAS* knockdown, but essentially no change in the case of *NRAS* knockdown (***Figure 4A-C***). By contrast, downregulation of both *KRAS* and *NRAS* reduced relative pAKT levels to a lesser extent, except on day 1 of differentiation. A profound effect was observed with the knockdown of *HRAS*, which essentially abrogated relative pAkt levels (***Figure 4D-F***). Taken together with the data above (***Figure 3***), we postulate distinct roles for the three Ras isoforms in regulating C2C12 differentiation (***Figure 4G***).

K-Ras4A/B proteins are important to maintain the Pax7+ progenitor pool and prevent differentiation of the transit amplifying cells (***Figure 3A-C***). N-Ras may have a similar and therefore partially redundant role, which is however obscured given that its downregulation unexpectedly upregulates K-Ras and to a lesser extent H-Ras (***Figure 3D-F***). This may correspond to a fail-safe mechanism, that makes sense in the context that *NRAS* is the evolutionary more recent Ras gene [71]. By contrast, H-Ras appears to promote terminal differentiation of the transit amplifying cells via the PI3K-pathway (***Figures 3I; 4F***). This pathway is however also impacted on by K-Ras4A/B and N-Ras on day 1 at the onset of differentiation (***Figure 4D-***

E). Both K-Ras4A/B and H-Ras predominantly sustain MAPK-signaling (***Figure 4A,C***), which may therefore be relevant for both progenitor maintenance by K-Ras4A/B (***Figure 3A***) and expansion of differentiated cells by H-Ras (***Figure 3F***).

Oncogenic K-Ras4B-G12V blocks differentiation of transit amplifying cells

It is well established that overactive MAPK-activity, such as associated with disease variants of pathway genes, blocks C2C12 cell differentiation [35,72]. However, it is unknown, in which subpopulation these defects manifest and whether proliferation is increased, as typically assumed for oncogenic Ras-transformed cells. Both oncogenic mutations as well as overexpression of Ras proteins is found in many cancers. Our flow cytometry-based differentiation assay offers the opportunity to exactly quantitate the expression level-dependent effect of both insults on differentiation, by gating for distinct transient expression levels of mEGFP-tagged wild-type or oncogenic K-Ras4B (hereafter K-Ras). Initially, 8,000 – 10,000 transfected cells were analyzed per condition, a number that remained constant until approximately day 2 of differentiation, when expression started to drop (***Figure 5-figure supplement 1A,B***). This transient perturbation of differentiation is necessary, as in stable transfectants the homeostasis of the mixed C2C12 cell pool would be permanently disrupted. For both constructs, most cells expressed in an expression window, which we defined as up to 10-fold above auto-fluorescence background of unlabeled cells (***Figure 5-figure supplement 1C,D***). A high-expression window essentially comprised all cells with expression levels beyond the former threshold.

In C2C12 cells expressing wt K-Ras in the low window, the fraction of Pax7+/ MyHC- progenitors remained essentially constant (***Figure 5A***), and at a comparable level to that of untransfected C2C12 cells (***Figure 1H***). As observed for untransfected C2C12 cells (***Figure 2A***), a decrease in the pool of transit amplifying Pax7-/ MyHC- cells (***Figure 5B***) was matched by an increase in the number of differentiated Pax7-/ MyHC+ cells (***Figure 5C***). Importantly, this fraction of differentiated cells was also comparable to the one found for non-transfected cells (***Figure 1H***), which suggests that the GFP low window corresponds to near physiological expression conditions.

By contrast, cells expressing wt K-Ras in the high window showed an increased fraction of progenitor cells (***Figure 5A***). High wt K-Ras expression then resulted in a decreased fraction of transit amplifying cells as compared to the low-expression window (***Figure 5B***), which was matched by a significantly increased fraction of differentiated cells that increased over time similar to cells expressing wt K-Ras in the GFP low expression window (***Figure 5C***), and non-transfected cells (***Figure 1H***).

A qualitatively different phenotype emerged with cells expressing K-RasG12V. From days 3-4, the fraction of progenitors appeared to slightly increase in the GFP low window and even more so in the high window (***Figure 5D***). At the same time, the fraction of transit amplifying cells transformed with K-RasG12V did not decrease (***Figure 5E***) as compared to cells expressing wt K-Ras (***Figure 5B***), irrespective of the

expression level. This was matched by a lack of the characteristic increase of differentiated cells from day 3 on (***Figure 5F***).

It is generally assumed that oncogenic Ras mutants increase proliferation, which could impact on the fractions of cells that are analyzed here. We therefore again performed dye-dilution experiments to determine the doubling times in the Pax7+ and Pax7- populations of cells transfected with mGFP-tagged wt K-Ras and K-RasG12V. Importantly, no significant differences were observed between the cytopainter dye dilution decay half-life values of wt K-Ras and K-RasG12V expressing cells in both the Pax7+ and Pax7- populations (***Figure 5G,H)***. We conclude that K-RasG12V imposes a differentiation block in the transit amplifying cells, while potentially increasing the numbers of progenitors (***Figure 5I***).

Oncogenic and RASopathy associated K-Ras mutants vary in their abilities to block differentiation

We next analyzed the impact of various Ras-pathway disease mutants on C2C12 cell differentiation. Again, we transiently transfected cells with mEGFP-tagged Ras-constructs and examined them by flow-cytometry in the GFP low window and at least 3000 cells were analyzed for each condition. We focused our analysis on day 3 of differentiation, as it is the earliest time point where differentiation measured by the fraction of MyHC+ cells become most significantly different between wt and oncogenic K-Ras in the GFP-low window (***Figure 5C, F***). In addition to the most frequent K-Ras mutations [73], we also included N-RasG12V and H-RasG12V for comparison.

While the Pax7+/ MyHC- progenitor pool remained nearly unaltered irrespective of which oncogenic Ras mutant was expressed (***Figure 6A***), their ability to block differentiation appeared to be distinct (***Figure 6B***). Also, N-RasG12V and H-RasG12V left the progenitor fraction unaltered (***Figure 6B***), while significantly blocking differentiation similar to the oncogenic K-Ras mutants (***Figure 6B***). Remarkably, the ability of the oncogenic K-Ras mutants to inhibit differentiation roughly followed the order of their mutation frequency in cancer, where K-RasG12D and K-RasG12C are the more frequent and K-RasQ61H is a less common mutation [73]. Exceptions were K-RasG13D and K-RasG12V, which are quite frequent, but had least blocking effect on differentiation.

Aberrant differentiation is also observed in developmental diseases called RASopathies, where Ras-pathway genes are mutated in the germline. Thus, every cell in the body would essentially experience malfunctioning Ras that could broadly impact on development. Consistently, all RASopathies are characterized by multi-organ abnormalities, including of the musculoskeletal system [74].

With a few exceptions, RASopathy mutations that are found in Ras are different from the ones seen in cancer [21,75]. RASopathy mutants typically display multiple biochemical abnormalities but have a milder effect on Ras-MAPK signaling than oncogenic mutants (***Table S1***) [22,63]. While the progenitor fractions were again hardly or rather negatively affected (***Figure 6C***), we saw in general a weaker or no ability of RASopathy-derived mutations to block differentiation (***Figure 6D***). The most obvious exception was K-Ras with the mutation G60R, which reached inhibition levels similar to those of the weakest oncogenic

mutant K-RasG13D. The third strongest RASopathy mutation in terms of inhibiting differentiation was K-RasP34R and on five came K-RasV14I. All of these mutants are characterized by a mild to substantial reduction in NF1-GAP sensitivity, a defect that is characteristic for all oncogenic mutants (***Table S1***) [22,76]. This points to a high significance of the NF1-GAP to facilitate terminal differentiation of transit amplifying cells.

K-RasG12C inhibitor profiling reveals their distinct ability to restore differentiation and induce toxic cell death

The past few years have seen the arrival of the first direct K-RasG12C inhibitors in the clinic [60,77]. Classical cell-based assays profile these inhibitors based on their anti-proliferative and cell-killing activity. Here, we have the unique opportunity to quantify to what extent these inhibitors can restore aberrant differentiation that was induced by oncogenic K-Ras alleles.

First, we established that the employed DMSO concentrations below 0.1 % that carried over from compound stocks do not impact on differentiation or have toxic effects (***Figure 7-figure supplement 1A,B)***. We then tested the two approved drugs sotorasib (AMG 510) and adagrasib (MRTX849) [56,78], as well as ARS-1620 the founder of current G12C-inhibitors [58] and MRTX1257, which is the less optimized tool compound of MRTX849. As just described, K-RasG12C decreased the fraction of MyHC+ cells more than K-RasG12V on day 3 (***Figure 7A***). AMG 510 treatment at 3 μM did not have a restorative effect on differentiation of cells expressing wt K-Ras or K-RasG12V, however, it significantly increased the fraction of differentiated cells with K-RasG12C even beyond that of the wt-control (***Figure 7A***). This was an interesting observations, as it may indicate a dominant negative action of AMG 510-bound K-RasG12C since this phenotype resembles that of the K-RasG12V-S17N (***Figure 7-figure supplement 1C,D***). This distinct ability of AMG 510 has not been reported previously. As expected, ARS-1620 could fully restore differentiation of K-RasG12C transformed C2C12 cells (***Figure 7B***), while having no effect on the number of intact cells as also observed with AMG 510 (***Figure 7-figure supplement 1E,F***). By contrast, neither MRTX1257 nor MRTX849 could fully restore differentiation of K-RasG12C transformed C2C12 cells (***Figure 7C,D***). Instead, we observed a reduction in the MyHC+ fraction in the drug treated K-RasG12V expressing cells (***Figure 7C,D***). This was due to significant general toxicity of these compounds, which led to a significant drop of intact cells even for wt K-Ras expressing cells (***Figure 7-figure supplement 1G,H***). We more closely examined this compound toxicity using 7-AAD-labelling, which indicates late apoptosis and necrosis in cells [79]. This assay confirmed that under otherwise the same conditions the general toxicity increased in the order AMG 510 $\lesssim$ ARS-1620 < MRTX1257 $\lesssim$ MRTX 849 in adherent and detached K-RasG12C transformed C2C12 cells (***Figure 7-figure supplement 1I,J***).

This analysis demonstrates that both AMG 510 and ARS-1620 are effective G12C inhibitors, which specifically restore differentiation without non-specific toxicity, while both MRTX1257 and MRTX 849 display a broader toxicity, which undermines their differentiation restoring ability.

Profiling of clinical and pre-clinical Ras inhibitors for their ability to restore differentiation.

In extension of this analysis, we next assessed the oncogene- and allele-specific effect of targeted drugs on differentiation. Altogether we tested eight approved or clinically evaluated Ras-pathway inhibitors at 1 μM (except for trametinib at 0.1 μM and AMG 510 at 3 μM), which target Ras trafficking (tipifarnib and cysmethynil), upstream activation (gefitinib, BI-3406), directly K-Ras (AMG 510, MRTX1133) and the major effector pathways downstream of Ras that are associated with cancer (trametinib, rapamycin).

Trafficking inhibitor tipifarnib, which inhibits farnesyl transferase, had a surprisingly broad effect on almost all K-Ras, N-Ras and H-Ras mutants to restore differentiation (***Figure 8A***). By contrast, cystmethynil was essentially ineffective (***Figure 8A***), in agreement with its clinical performance [80]. The expected H-Ras specificity of tipifarnib treatment becomes more clearly visible, if we consider the net rescue effect of differentiation, i.e. the difference between the MyHC+ fraction with drug treatment and the DMSO-control (***Figure 8B***). The second most sensitive allele was N-RasG12V, interestingly followed by K-RasG12V, while all other oncogenic K-Ras variants were less sensitive. This was surprising, given that K- and N-Ras can undergo alternative prenylation if farnesyltransferase is inhibited [81].

Upstream inhibitors gefitinib, which blocks EGFR tyrosine kinase activity, only had a modest increase to restore differentiation for some K-Ras alleles (***Figure 8A,B***), which essentially followed the order of the differentiation blocking activity of these K-Ras mutants (***Figure 6B***). The SOS1 inhibitor BI-3406 fared better, leading to a substantial restoration, except for K-RasQ61H, which is known to have a high intrinsic nucleotide exchange activity that allows its activation independent from SOS1 [82,83].

Next, AMG 510 showed the expected selectivity for K-RasG12C, with a minor effect on other alleles (K-RasG13D, K-RasG12V and N-RasG12V) (***Figure 8A,B***). Allele selectivity, albeit not as clear as with AMG 510, was also seen with the low nanomolar non-covalent K-RasG12D-selective inhibitor MRTX1133 [59]. Importantly, MRTX1133 restored differentiation to the highest levels observed so far for K-RasG12D but did appear to also mildly and non-specifically increase the differentiated fraction in other K-Ras alleles (***Figure 8A,B***). These apparent non-specific effects of the two allele specific inhibitors may arise from interactions with the switch II pocket on all K-Ras alleles. For compounds with the MRTX849 scaffold such non-specificity was explicitly demonstrated earlier [84].

None of the former compounds though exerted an as strong pan-Ras effect as trametinib, which broadly restored differentiation across all alleles and isoforms (***Figure 8A,B***). However, drugs that have a known allele- or isoform-selectivity (tipifarnib for H-RasG12V, AMG 510 for K-RasG12C and MRTX1133 for K-RasG12D) matched or surpassed the effect of trametinib. This correlated with the clinical success of tipifarnib against H-RasG12V driven tumors and of AMG 510 against K-RasG12C driven tumors [85,86].

We, therefore, not only demonstrate an approximate correlation between the strength of each mutant to block differentiation with its observed clinical frequency but also recapitulate the *in vivo* effects of pharmacological agents. The broad effect of trametinib moreover highlights the central role of the MAPK

pathway to block differentiation. It was surprising to see that both N-RasG12V and H-RasG12V were having a similar potential to block differentiation as several K-Ras alleles, including K-RasG12V, that are mutated at a higher frequency (***Figure 8C***).

Our knockdown data suggested that H-Ras sustains both MAPK- and PI3K-pathway activity, while K-Ras4A/B mostly impact on MAPK-activity during differentiation (***Figure 4G***). Yet, K-Ras loss increased the fraction of differentiated cells (***Figure 3C***), suggesting that the MAPK-activity associated with it was inhibitory for differentiation (**Figure 8D**). One would therefore expect that PI3K-inhibition by rapamycin blocks differentiation that is perturbed by oncogenic H-RasG12V. Indeed, this was the case, but also seen for K-RasG12V and N-RasG12V (***Figure 8E***). We therefore hypothesized that the latter two oncogenes upregulate the PI3K pathway, unlike their wt counterparts (***Figure 8F***). This would have profound consequences, as in that case inhibition of the MAPK-pathway by trametinib would leave the PI3K-pathway intact to sustain differentiation (***Figure 8F***).

This explains, why trametinib broadly restores differentiation across all oncogenic Ras alleles (***Figure 8B***). One would expect a stronger effect of trametinib on the Ras isoform that is naturally wired to activate the MAPK- and PI3K-pathway (**Figure 8D**), namely H-Ras. When looking at differentiation data of cells transformed with the three oncogenic Ras isoforms treated with trametinib, this is not entirely obvious (***Figure 8G***). However, when the net restoration of differentiation by trametinib is considered i.e., the difference between the MyHC+ fraction with drug treatment and the DMSO-control, the higher sensitivity of H-RasG12V transformed cells to restoration by trametinib and lower sensitivity of K-RasG12V-transformed cells, which only acquired PI3K-activation in the oncogenic setting, becomes apparent (***Figure 8H***).

Considering that N-RasG12V behaves similar to H-RasG12V in terms of trametinib sensitivity, we would also hypothesize that its wt counterpart naturally signals both via the MAPK- and PI3K-pathways. However, given the upregulation of K-Ras4A/B and H-Ras upon *NRAS* knockdown, this may have remained hidden (***Figure 4B,E***). Intriguingly, the same order of sensitivity was found for tipifarnib (***Figure 8B***), which may indicate that both drugs, tipifarnib and trametinib could work synergistically to block differentiation. By contrast, the inverse was seen for the treatment with rapamycin (***Figure 8 B***), suggesting that those mutants that have the strongest MAPK-dependence, have the least PI3K-dependence for their blocking effect on differentiation. When the net restoration of other oncogenic K-Ras alleles by trametinib is analyzed (***Figure 8I***), one recovers a rank-order that anti-correlates with the impact of these alleles on differentiation (***Figure 6B***).

Discussion

The impact of Ras-MAPK-pathway disease mutants on cell transformation and the efficacy of novel Ras drug candidates are typically assessed in a small number of standard assays, such as NIH3T3 transformation

and 2D/3D cancer cell proliferation assays, complemented by immunoblotting for markers of Ras-MAPK-pathway activity [87]. The impact on cell differentiation, though a known hallmark of cancer, has so far been vastly neglected.

Here we have established the C2C12 cell model to examine the effect of oncogenic Ras mutants and Ras-pathway drugs on differentiation. Importantly, this model recapitulates typical and fundamental steps of cell differentiation also found in vivo [38]. This suggests that our observations have broad implications not only for locally perturbed differentiation in cancer, but also for RASopthies, which are caused by aberrant Ras signaling throughout development. Our approach with a standard commercial cell line is advantageous as compared to the usage of human embryonic stem cells (hESC), which have also been used to identify compounds that maintain stemness or promote differentiation in more laborious, imaging-based high content screens [88-91].

Based on our analysis, we propose a new model how in the C2C12 cell culture a small proportion of Pax7+ progenitor myoblasts are maintained, while the majority of cells is prone to differentiate (***Figure 4G***). We found that frequent asymmetric divisions maintain the Pax7+/ MyHC- progenitor pool, while generating a transit amplifying Pax7-/ MyHC- pool of cells that exponentially expands within a few symmetric divisions. We show here that the three cancer associated Ras genes, *KRAS*, *NRAS* and *HRAS* have a distinct, yet partially overlapping involvement in sustaining the proper trajectory from progenitors via here identified transit amplifying cells to differentiated cells. Individual knockdowns generate distinct patterns of changes that are incompatible with the alternative explanation that total Ras levels determine the alterations. Our data suggest a particular relevance of K-Ras4A/B-dependent MAPK-signaling for progenitor maintenance and H-Ras-dependent PI3K-signaling for terminal differentiation. Lowering the MAPK-output drives differentiation in the transit amplifying pool when adequate levels of PI3K-activity is present. This is consistent with previous reports of MAPK inhibition resulting in increased differentiation [92]. Our model contrasts to currently debated models for the isoform specific functions of these Ras genes, that include differences in plasma membrane segregation and effector usage. The generally observed high expression level in particular of K-Ras4B in almost all tissues is consistent with its major function to sustain progenitors and being the evolutionary most ancient Ras isoform [6,71].

It is well established that oncogenic Ras, constitutively active Raf or MEK1 inhibit myoblast differentiation [93-95]. However, we observed two distinct types of perturbed differentiation by Ras-pathway hyperactivation. The first is associated with overexpression of K-Ras that led to a more pronounced drop in the transit amplifying population but significantly increased differentiation. We speculate this is due to a spill-over of K-Ras activity into the PI3K-pathway, similar to what is observed for the oncogenic mutant. Qualitatively different, oncogenic K-RasG12V blocks terminal differentiation of transit amplifying cells, without increasing the proliferation as compared to wt K-Ras. Indeed, all seven here examined NF1-GAP

insensitive oncogenic Ras variants block differentiation, however, those mutants that show here a stronger dependence on MAPK-signaling, such as K-RasG12D, are more potent to block differentiation. As already inferred from their biochemical characterization, RASopathy associated K-Ras mutants are not or less able to block differentiation, consistent with these alterations being compatible with organismal development. Instead, it appears that many of them are defective in sustaining the progenitor fraction. Intriguingly, the most potent RASopathy mutant K-RasG60R, which inhibits differentiation as much as the weakest oncogenic K-Ras allele K-RasG13D, also displays a more prominent NF1-GAP resistance. The milder effects of RASopathy K-Ras mutants G60R and P34R can be explained by their decreased effector engagement, which also exists in a milder manifestation in the V14I mutant.

We speculate that for all of these NF1-GAP resistant mutants, differentiation of transit amplifying cells is blocked, as shown for K-RasG12V. This is consistent with the fact that with the induction of differentiation, the potentially K-Ras-selective tumor suppressor complex of SPRED1 with the GAP NF1 can form after SPRED1-induction [10,12,35]. Thus, MAPK-signaling would be sustained in transit amplifying cells, which prevents differentiation. This specifies that the oncogenic insult of hotspot-mutated Ras occurs at a defined point of the differentiation trajectory, an important fact that has not been recognized before. Moreover, our data suggest molecular mechanistic and developmental commonalities between cancer and RASopathies, which have been long elusive.

In direct correlation with our muscle cell line observations, RASopathy patients display muscle weakness in particular in Costello syndrome (CS) [74,96]. In the heterozygous G12V CS mouse model a decreased muscle mass and strength was found, due to inhibited embryonic myogenesis and myofiber formation [97]. This was due to an inhibited differentiation in the embryonic muscles, with a 23 % increase in Pax7 expressing cells and a decrease in MyoD and myogenin expressing cells to 60-70 % of the wt. A less severe skeletal myopathy is observed in the RASopathy cardiofaciocutaneous syndrome mouse model with a BRAF-L597V mutation [98]. Given the distinct penetrance of muscle phenotypes in RASopathies, one may assume this could be due to distinct mutant allele strengths, as suggested by our data. Alternatively, in muscle cells only certain alleles become significant, while others are tissue specifically contained, probably a less likely scenario.

Importantly, these data corroborate the idea that the muscle phenotype in RASopathies is due to perturbed differentiation of stem/ progenitor cells, as has been observed in other muscle diseases notably in Duchenne muscular dystrophy where asymmetric cell divisions of satellite cells are likewise not proceeding correctly [99].

Also cancer is associated with muscle wasting caused by the hyperactivation of the Ras-MAPK [100,101]. And last but not least, soft tissue rhabdomyosarcoma (RMS) of the muscle are frequently observed in RASopathies, such as Neurofibromatosis type 1, Noonan syndrome and CS [102]. RMS is the most common childhood soft-tissue sarcoma with only 30 % survival in the metastatic disease. These tumors emerge from

muscle progenitors/ myoblasts that failed to differentiate, albeit the exact cell of origin is still not well characterized [102]. Strikingly, this is exactly the phenotype we have observed in our data. Two subtypes are distinguished, the alveolar type in adolescents and the embryonal type in younger patients is associated with good prognosis, despite higher mutational burden [103]. The former largely overlaps with the Pax-fusion positive molecular subtype, with neomorphic gain of function fusion proteins of Pax3 or Pax7 with FOXO1. In the Pax-fusion negative (embryonal) subtype of RMS, the Ras-pathway is activated by mutations in the pathway, while in the Pax-fusion positive subtype the upregulation of pathway genes is found [102,103]. Interestingly, it is one of the few cancer types where the three Ras isoforms are mutated at about equal frequency. However, NRAS more often in adolescents, while KRAS and HRAS mutations more frequently occur in infants. In line with our observations, oncogenic Ras prevents differentiation in rhabdomyosarcoma [104].

Finally, we profiled the effect of drugs on differentiation in a rapid and insightful manner. Our assessment of four K-Ras-G12C inhibitors importantly demonstrates that inhibition of the oncogenic K-Ras also rescues differentiation. Yet, unexpected idiosyncrasies of these compounds were observed. Interestingly, the increase in differentiation that we observed with K-RasG12C bound AMG 510, may suggest a molecular complex that becomes dominant negative, similar to what is seen with K-RasS17N. It is not likely that target-independent, off-target effects are responsible for this observation, as there is no effect with K-RasG12V expressing cells. By contrast, adagrasib (MRTX849) and more so MRTX1257 were less proficient in restoring differentiation, while inducing significantly more non-specific cell death. This is typically not desired, and in this particular case it may be attributed to the inhibition of wt K-Ras and possibly other mutant *KRAS* alleles [84]. This is beneficial in the clinical setting, where any antiproliferative activity could be helpful and the activity against other *KRAS* alleles prevents their success if they emerge as a resistance mechanism.

Consistent with observations in the more complex hESC model and zebra fish larvae [105,106], we also noted the significant, dose-dependent effect of DMSO at concentrations above 0.5 % on C2C12 cell differentiation (**Figure SI**). Hence, our assay may be suitable to identify and explain differentiation perturbing, toxic effects of organic solvents or other substances that may correlate with their teratogenic potential.

We furthermore illustrate the enormous potential for Ras-pathway drug profiling on Ras-disease mutants in our 8 × 8 matrix, which revealed a remarkable correlation of the ability of drugs to restore differentiation with their clinical efficacy in Ras disease treatment. The broad capacity to restore differentiation by MEK-inhibition is paralleled by results obtained with myocyte cultures derived from the CS mouse model. Differentiation of those cells could be restored by the MEK inhibitor PD0325901, while in the WT control differentiation was further increased. Importantly, this was mirrored by muscle-mass and -diameter

increases in vivo to control levels [97]. Thus, relative muscle strength development in RASopathy patients may also serve as a biomarker for treatment efficacy. We found that rapamycin was one of the few compounds, which prevented C2C12 cell differentiation (***Figure 8A***), in line with findings by others [107]. While the PI3K/Akt/ mTORC1/S6K1-axis is involved in hypertrophic muscle growth [108,109], the PI3K inhibitor GDC0941 led to muscle cell death in a CS mouse model and was deleterious in vivo [97]. However, in the aging muscle, hyperactive mTORC1 appears to induce muscle damage and loss, hence low dose treatment with rapamycin analogue everolimus (RAD001) salvages this situation in vivo [110].

In the end, this compound analysis allowed us to derive a simplified signaling model that explains how the differences in MAPK- and PI3K-pathway activation in particular of K-Ras and H-Ras give rise to distinct drug responses of pathway inhibitors. Future developments of such drug-profiling derived models may enable us to predict efficacious drug combination that do not only restore differentiation but in parallel also work in cancer therapy.

The fact that we observe striking correlations of our differentiation data with overall Ras mutation strength and drug-responses observed in the clinic, suggests that we are looking here at a highly conserved activity of Ras that is deeply engrained into the functioning of every cell system. In order to devise therapies that can fully salvage the aberrant differentiation induced by Ras-pathway hyperactivation, we need to understand its impact on both cell proliferation and differentiation. The involvement of Ras beyond the G1-phase, where the Ras-MAPK pathway is known to drive S-phase entry by stimulating cyclin D expression, is largely unknown. However, cell fate decisions are taken during M-phase, as stem/ progenitor cells symmetrically or asymmetrically divide. We postulate a distinct role of Ras-pathway activity during this fundamental step, which cannot merely be explained by different strengths of the pathway output, but the underlying cell and developmental biology.

Figure legends

Figure 1. Improved characterization of C2C12 cell differentiation by flow cytometry.

(**A**) Differentiation of skeletal muscle *in vivo* (top) and of C2C12 cells (bottom) are similar based on marker expression.

(**B**) C2C12 cells were differentiated by switching to low serum medium for indicated times. Brightfield images were obtained at 20 × magnification. Scale bars, 200 µm.

(**C-H**) Representative immunoblots and quantification of Pax7 (C), myogenin (E) and MyHC (G) expression in C2C12 cells; N = 3. Representative flow cytometry histograms of marker+ cells at indicated times after serum switch (left). Quantification of marker+ fraction and geometric means of intensities (right). Analyzed markers were Pax7 (D), myogenin (F) and MyHC (H); N = 3. Statistical significance was calculated using the Friedman's test and Dunn's post hoc test in comparison to d0. The switch to low serum medium for differentiation is here and in the following indicated with a vertical dashed line.

Figure 2. A major pool of Pax7-/ MyHC- transit amplifying cells gives rise to Pax7-/ MyHC- differentiated cells.

(**A**) Flow cytometric analysis of C2C12 cell subpopulations after indicated times of differentiation; N = 3. Numbers above bars give cell percentages.

(**B,C**) Quantification of mitotically active (pH3+) Pax7+ (B) and Pax7- (C) subpopulations; N = 4.

(**D**) Representative histograms of cytopainter dye dilution experiments from C2C12 cells proliferating in high serum medium for indicated times.

(**E**) Quantification of dye dilution experiments as in (D). Geometric means of fluorescence intensities of cytopainter deep red-labelled Pax7+ and Pax7- cells; N = 3. Half-life ($t_{1/2}$) of each fluorescence decay was calculated as described in methods.

(**F**) Analysis of cell concentrations of Pax7+ and Pax7- populations proliferating in high serum; N = 3.

(**G**) Revised population model for C2C12 cells. Our data suggest that Pax7+/ MyHC- progenitors divide asymmetrically to maintain their pool and expand the number of slowly proliferating Pax7-/ MyHC- transit amplifying cells, which make up the major pool of cells that differentiate into Pax7-/ MyHC+ cells in low serum.

Figure 3. K-Ras4A/4B block whereas H-Ras promotes C2C12 differentiation.

(**A-I**) Flow cytometric quantification of double-labelled C2C12 cells at indicated times of differentiation. At day 0 cells were treated with si*KRAS* to knock down both isoforms K-Ras4A/4B or control siRNA (CTRL) (A-C). Analogous treatments were done using si*NRAS* (D-F) or si*HRAS* (G-I).

Then the fractions of Pax7+/ MyHC- progenitors (A,D,G), Pax7-/ MyHC- transit amplifying cells (B,E,H) and Pax7-/ MyHC+ differentiated cells (C,F,I) were determined by flow cytometric analysis. Ideograms of

cells at the top indicate the analyzed cell population in the column of panels; N ≥ 4. The numbers above the bars show percentages. A line (not shown) was fit to each of the plots to indicate the altered trend in cell fractions by their slope values.

Figure 4. K-Ras4A/4B sustain MAPK-signaling, while H-Ras sustains both MAPK- and PI3K-signalling during differentiation.

(**A-C**) Representative immunoblots of C2C12 cell lysates (top) and their quantified normalized pERK signals after knockdown of *KRAS* (A), *NRAS* (B) and *HRAS* (C) at day 0; N = 2.

(**D-F**) Representative immunoblots of C2C12 cell lysates (top) and their quantified normalized pAkt signals after knockdown of *KRAS* (D), *NRAS* (E) and *HRAS* (F); N = 2.

(**G**) Update of our population model for C2C12 cell differentiation with inferred participation of Ras isoforms in cell divisions and their contribution to MAPK- and PI3K-pathway activity indicated on the left.

Figure 5. Oncogenic K-Ras4B blocks differentiation of transit amplifying cells.

(**A-C**) Flow cytometric analysis of temporal evolution of Pax7+/ MyHC- progenitors (A), Pax7-/ MyHC- transit amplifying cells (B) and Pax7-/ MyHC+ differentiated cells (C) after transfection of C2C12 cells with mEGFP tagged wt K-Ras on day 0. Cells in the GFP-low and GFP-high expression windows were analyzed; N = 2.

(**D-F**) Flow cytometric analysis of temporal evolution of Pax7+/ MyHC- progenitors (D), Pax7-/ MyHC- transit amplifying cells (E) and Pax7-/ MyHC+ differentiated cells (F) after transfection of C2C12 cells with mEGFP tagged oncogenic K-RasG12V on day 0. Cells in the GFP-low and GFP-high expression windows were analyzed; N = 2.

(**G,H**) Geometric means of fluorescence intensities of cytopainter orange-labelled Pax7+ (G) and Pax7- (H) of mEGFP-wt K-Ras or mEGFP-K-RasG12V expressing C2C12 cells; N = 3. Half-life ($t_{1/2}$) of each fluorescence decay was calculated as described in methods.

(**I**) Population model for C2C12 cells transformed with oncogenic K-RasG12V, which blocks differentiation at the level of Pax7-/ MyHC- transit amplifying cells.

Figure 6. All oncogenic Ras mutants block differentiation, while RASopathy associated K-Ras mutants affect differentiation more broadly. (**A,B**) EGFP-variant tagged oncogenic Ras constructs were transfected into C2C12 cells on day 0 and subsequently on day 3 of differentiation Pax7+ cell fractions (A) and MyHC+ cell fractions (B) were analzed by flow cytometry; N = 3.

(**C,D**) EYFP-tagged K-Ras RASopathy mutants were transfected into C2C12 cells on day 0 and subsequently on day 3 of differentiation Pax7+ cell fractions (A) and MyHC+ cell fractions (B) were analzed by flow cytometry; N = 3.

In all plots, only cells in the GFP-low expression windows were analyzed.

Figure 7. K-RasG12C inhibitor profiling reveals their distinct ability to restore differentiation.
(**A-D**) Analysis of MyHC+ C2C12 cell fractions expressing GFP-variant tagged wt K-Ras, K-RasG12V and K-RasG12C on day 3 of differentiation. From day 1 onwards 3 μM of AMG 510 (A), ARS-1620 (B), MRTX1257 (C) or MRTX849 (D) or vehicle (DMSO 0.1 % v/v) were added to cells; N = 3.
In all plots, only cells in the GFP-low expression windows were analyzed.

Figure 8. Profiling of clinically tested Ras inhibitors for their ability to restore differentiation.
(**A**) Heatmap showing % MyHC+ C2C12 cells on day 3 of differentiation for each indicated condition. EGFP-variant tagged Ras-constructs were transfected on day 0; N = 3. The scale to the right shows the wt K-Ras differentiation level as a reference.
(**B**) Net rescue effect of drugs. Data from (A) were used by subtracting values from vehicle control (DMSO 0.2 % v/v) treated samples in the top row from those treated with drugs. The scale to the right shows the DMSO-control effect as a reference.
(**C**) Extract of data from (A) showing MyHC+ C2C12 cell fraction of indicated EGFP-variant tagged Ras-constructs with vehicle treatment.
(**D**) Schematic showing modulation of MAPK and PI3K pathways downstream of wt H-Ras and wt K-Ras4A/4B, based on **Figure 4** data.
(**E**) Extract of data from (A) showing MyHC+ C2C12 cell fraction of indicated EGFP-variant tagged Ras-constructs with 1μM rapamycin treatment.
(**F**) Schematic showing hypothesized effect of oncogenic H-RasG12V and K-RasG12V on MAPK and PI3K pathways.
(**G**) Extract of data from (A) showing MyHC+ C2C12 cell fraction of indicated EGFP-variant tagged Ras-constructs with 0.1 μM trametinib treatment.
(**H**) Extract of data from (B). Net rescue effect of trametinib treatment indicates dependence of indicated Ras-proteins on MAPK-pathway.
(**I**) Extract of data from (B) MAPK-pathway dependence of K-Ras variants judged by the trametinib induced net rescue.
In all plots, only cells in the GFP-low expression windows were analyzed.

Resource availability

Further information and requests for resources and reagents should be directed to and will be fulfilled by the lead contact, Daniel Kwaku Abankwa (daniel.abankwa@uni.lu).

Acknowledgements

This work was supported by a grant from the Luxembourg National Research Fund (FNR) grant C19/BM/13673303-PolaRAS2 to D.K.A.

Author contributions

R.C. and D.A. conceptualized the study.

R.C. and B.P. designed and carried out most of the experiments.

F.K., C.L. and N. B.F. performed supplementary experiments.

R.C. and B.P. analyzed the data.

R.C. and B.P. wrote the first draft of the manuscript. D.K.A. finalized the manuscript and supervised the entire study.

Declaration of interests

The authors declare no competing interests.

Supplementary Information

Supplementary Data are part of this study and are uploaded separately.

References

1. Crespo, P., and Leon, J. (2000). Ras proteins in the control of the cell cycle and cell differentiation. Cell Mol Life Sci *57*, 1613-1636. 10.1007/pl00000645.

2. Hanahan, D., and Weinberg, R.A. (2011). Hallmarks of cancer: the next generation. *144*, 646-674. papers3://publication/doi/10.1016/j.cell.2011.02.013.

3. Prior, I.A., Hood, F.E., and Hartley, J.L. (2020). The Frequency of Ras Mutations in Cancer. Cancer Res *80*, 2969-2974. 10.1158/0008-5472.CAN-19-3682.

4. Moore, A.R., Rosenberg, S.C., McCormick, F., and Malek, S. (2020). RAS-targeted therapies: is the undruggable drugged? Nat Rev Drug Discov *19*, 533-552. 10.1038/s41573-020-0068-6.

5. Tsai, F.D., Lopes, M.S., Zhou, M., Court, H., Ponce, O., Fiordalisi, J.J., Gierut, J.J., Cox, A.D., Haigis, K.M., and Philips, M.R. (2015). K-Ras4A splice variant is widely expressed in cancer and uses a hybrid membrane-targeting motif. Proc Natl Acad Sci U S A *112*, 779-784. 10.1073/pnas.1412811112.

6. Hood, F.E., Sahraoui, Y.M., Jenkins, R.E., and Prior, I.A. (2023). Ras protein abundance correlates with Ras isoform mutation patterns in cancer. Oncogene *42*, 1224-1232. 10.1038/s41388-023-02638-1.

7. Pavic, K., Chippalkatti, R., and Abankwa, D. (2022). Drug targeting opportunities en route to Ras nanoclusters. Adv Cancer Res *153*, 63-99. 10.1016/bs.acr.2021.07.005.

8. Schmick, M., Kraemer, A., and Bastiaens, P.I. (2015). Ras moves to stay in place. Trends Cell Biol *25*, 190-197. 10.1016/j.tcb.2015.02.004.

9. Simanshu, D.K., Nissley, D.V., and McCormick, F. (2017). RAS Proteins and Their Regulators in Human Disease. Cell *170*, 17-33. papers3://publication/doi/10.1016/j.cell.2017.06.009.

10. Stowe, I.B., Mercado, E.L., Stowe, T.R., Bell, E.L., Oses-Prieto, J.A., Hernandez, H., Burlingame, A.L., and McCormick, F. (2012). A shared molecular mechanism underlies the human rasopathies Legius syndrome and Neurofibromatosis-1. Genes Dev *26*, 1421-1426. 10.1101/gad.190876.112.

11. Yan, W., Markegard, E., Dharmaiah, S., Urisman, A., Drew, M., Esposito, D., Scheffzek, K., Nissley, D.V., McCormick, F., and Simanshu, D.K. (2020). Structural Insights into the SPRED1-Neurofibromin-KRAS Complex and Disruption of SPRED1-Neurofibromin Interaction by Oncogenic EGFR. Cell Rep *32*, 107909. 10.1016/j.celrep.2020.107909.

12. Siljamaki, E., and Abankwa, D. (2016). SPRED1 Interferes with K-ras but Not H-ras Membrane Anchorage and Signaling. Mol Cell Biol *36*, 2612-2625. 10.1128/MCB.00191-16.

13. Scheffzek, K., Ahmadian, M.R., Kabsch, W., Wiesmuller, L., Lautwein, A., Schmitz, F., and Wittinghofer, A. (1997). The Ras-RasGAP complex: structural basis for GTPase activation and its loss in oncogenic Ras mutants. Science *277*, 333-338. 10.1126/science.277.5324.333.

14. Ahmadian, M.R., Stege, P., Scheffzek, K., and Wittinghofer, A. (1997). Confirmation of the arginine-finger hypothesis for the GAP-stimulated GTP-hydrolysis reaction of Ras. Nat Struct Biol *4*, 686-689. 10.1038/nsb0997-686.

15. Li, C., Vides, A., Kim, D., Xue, J.Y., Zhao, Y., and Lito, P. (2021). The G protein signaling regulator RGS3 enhances the GTPase activity of KRAS. Science *374*, 197-201. 10.1126/science.abf1730.

16. Tsherniak, A., Vazquez, F., Montgomery, P.G., Weir, B.A., Kryukov, G., Cowley, G.S., Gill, S., Harrington, W.F., Pantel, S., Krill-Burger, J.M., et al. (2017). Defining a Cancer Dependency Map. Cell *170*, 564-576 e516. 10.1016/j.cell.2017.06.010.

17. McDonald, E.R., 3rd, de Weck, A., Schlabach, M.R., Billy, E., Mavrakis, K.J., Hoffman, G.R., Belur, D., Castelletti, D., Frias, E., Gampa, K., et al. (2017). Project DRIVE: A Compendium of Cancer Dependencies and Synthetic Lethal Relationships Uncovered by Large-Scale, Deep RNAi Screening. Cell *170*, 577-592 e510. 10.1016/j.cell.2017.07.005.

18. Barretina, J., Caponigro, G., Stransky, N., Venkatesan, K., Margolin, A.A., Kim, S., Wilson, C.J., Lehar, J., Kryukov, G.V., Sonkin, D., et al. (2012). The Cancer Cell Line Encyclopedia enables predictive modelling of anticancer drug sensitivity. Nature *483*, 603-607. 10.1038/nature11003.

19. Chaffer, C.L., and Weinberg, R.A. (2015). How does multistep tumorigenesis really proceed? Cancer Discov *5*, 22-24. 10.1158/2159-8290.CD-14-0788.

20. Rauen, K.A. (2013). The RASopathies. Annu Rev Genomics Hum Genet *14*, 355-369. 10.1146/annurev-genom-091212-153523.

21. Castel, P., Rauen, K.A., and McCormick, F. (2020). The duality of human oncoproteins: drivers of cancer and congenital disorders. Nat Rev Cancer *379*, 1-15. papers3://publication/doi/10.1038/s41568-020-0256-z.

22. Gremer, L., Merbitz-Zahradnik, T., Dvorsky, R., Cirstea, I.C., Kratz, C.P., Zenker, M., Wittinghofer, A., and Ahmadian, M.R. (2011). Germline KRAS mutations cause aberrant biochemical and physical properties leading to developmental disorders. Hum Mutat *32*, 33-43. 10.1002/humu.21377.

23. Brems, H., Pasmant, E., Van Minkelen, R., Wimmer, K., Upadhyaya, M., Legius, E., and Messiaen, L. (2012). Review and update of SPRED1 mutations causing Legius syndrome. Hum Mutat *33*, 1538-1546. 10.1002/humu.22152.

24. Jindal, G.A., Goyal, Y., Burdine, R.D., Rauen, K.A., and Shvartsman, S.Y. (2015). RASopathies: unraveling mechanisms with animal models. Dis Model Mech *8*, 769-782. 10.1242/dmm.020339.

25. Gross, A.M., Frone, M., Gripp, K.W., Gelb, B.D., Schoyer, L., Schill, L., Stronach, B., Biesecker, L.G., Esposito, D., Hernandez, E.R., et al. (2020). Advancing RAS/RASopathy therapies: An NCI-sponsored intramural and extramural collaboration for the study of RASopathies. Am J Med Genet A *182*, 866-876. 10.1002/ajmg.a.61485.

26. Morrison, S.J., and Kimble, J. (2006). Asymmetric and symmetric stem-cell divisions in development and cancer. Nature *441*, 1068-1074. 10.1038/nature04956.

27. Altshuler, A., Verbuk, M., Bhattacharya, S., Abramovich, I., Haklai, R., Hanna, J.H., Kloog, Y., Gottlieb, E., and Shalom-Feuerstein, R. (2018). RAS Regulates the Transition from Naive to Primed Pluripotent Stem Cells. Stem Cell Reports *10*, 1088-1101. 10.1016/j.stemcr.2018.01.004.

28. Haghighi, F., Dahlmann, J., Nakhaei-Rad, S., Lang, A., Kutschka, I., Zenker, M., Kensah, G., Piekorz, R.P., and Ahmadian, M.R. (2018). bFGF-mediated pluripotency maintenance in human induced pluripotent stem cells is associated with NRAS-MAPK signaling. Cell Commun Signal *16*, 96. 10.1186/s12964-018-0307-1.

29. Bennett, A.M., and Tonks, N.K. (1997). Regulation of distinct stages of skeletal muscle differentiation by mitogen-activated protein kinases. Science *278*, 1288-1291. 10.1126/science.278.5341.1288.

30. Yoshida, N., Yoshida, S., Koishi, K., Masuda, K., and Nabeshima, Y. (1998). Cell heterogeneity upon myogenic differentiation: down-regulation of MyoD and Myf-5 generates 'reserve cells'. J Cell Sci *111 (Pt 6)*, 769-779. 10.1242/jcs.111.6.769.

31. Brown, D.M., Parr, T., and Brameld, J.M. (2012). Myosin heavy chain mRNA isoforms are expressed in two distinct cohorts during C2C12 myogenesis. J Muscle Res Cell Motil *32*, 383-390. 10.1007/s10974-011-9267-4.

32. Olguin, H.C., and Olwin, B.B. (2004). Pax-7 up-regulation inhibits myogenesis and cell cycle progression in satellite cells: a potential mechanism for self-renewal. Dev Biol *275*, 375-388. 10.1016/j.ydbio.2004.08.015.

33. Parisi, B., Sünnen, M., Chippalkatti, R., and Abankwa, D.K. (2023). A flow-cytometry-based pipeline for the rapid quantification of C2C12 cell differentiation. STAR Protoc, 102637. 10.1016/j.xpro.2023.102637.

34. Yablonka-Reuveni, Z., and Rivera, A.J. (1994). Temporal expression of regulatory and structural muscle proteins during myogenesis of satellite cells on isolated adult rat fibers. Dev Biol *164*, 588-603. 10.1006/dbio.1994.1226.

35. Wakioka, T., Sasaki, A., Kato, R., Shouda, T., Matsumoto, A., Miyoshi, K., Tsuneoka, M., Komiya, S., Baron, R., and Yoshimura, A. (2001). Spred is a Sprouty-related suppressor of Ras signalling. Nature *412*, 647-651. 10.1038/35088082.

36. Lassar, A.B., Thayer, M.J., Overell, R.W., and Weintraub, H. (1989). Transformation by activated ras or fos prevents myogenesis by inhibiting expression of MyoD1. Cell *58*, 659-667. 10.1016/0092-8674(89)90101-3.

37. de Alvaro, C., Martinez, N., Rojas, J.M., and Lorenzo, M. (2005). Sprouty-2 overexpression in C2C12 cells confers myogenic differentiation properties in the presence of FGF2. Mol Biol Cell *16*, 4454-4461. 10.1091/mbc.e05-05-0419.

38. Yin, H., Price, F., and Rudnicki, M.A. (2013). Satellite cells and the muscle stem cell niche. Physiol Rev *93*, 23-67. 10.1152/physrev.00043.2011.

39. Ansieau, S. (2013). EMT in breast cancer stem cell generation. Cancer Letters *338*, 63-68. 10.1016/j.canlet.2012.05.014.

40. Batlle, E., and Clevers, H. (2017). Cancer stem cells revisited. Nat Med *23*, 1124-1134. 10.1038/nm.4409.

41. Nassar, D., and Blanpain, C. (2016). Cancer Stem Cells: Basic Concepts and Therapeutic Implications. Annu Rev Pathol *11*, 47-76. papers3://publication/doi/10.1146/annurev-pathol-012615-044438.

42. Golebiewska, A., Brons, N.H., Bjerkvig, R., and Niclou, S.P. (2011). Critical appraisal of the side population assay in stem cell and cancer stem cell research. Cell Stem Cell *8*, 136-147. 10.1016/j.stem.2011.01.007.

43. Li, W., Ma, H., Zhang, J., Zhu, L., Wang, C., and Yang, Y. (2017). Unraveling the roles of CD44/CD24 and ALDH1 as cancer stem cell markers in tumorigenesis and metastasis. Sci Rep *7*, 13856. 10.1038/s41598-017-14364-2.

44. Dontu, G., Abdallah, W.M., Foley, J.M., Jackson, K.W., Clarke, M.F., Kawamura, M.J., and Wicha, M.S. (2003). In vitro propagation and transcriptional profiling of human mammary stem/progenitor cells. Genes Dev *17*, 1253-1270. 10.1101/gad.1061803.

45. Weiswald, L.B., Bellet, D., and Dangles-Marie, V. (2015). Spherical cancer models in tumor biology. Neoplasia *17*, 1-15. 10.1016/j.neo.2014.12.004.

46. She, X., Gao, Y., Zhao, Y., Yin, Y., and Dong, Z. (2021). A high-throughput screen identifies inhibitors of lung cancer stem cells. Biomed Pharmacother *140*, 111748. 10.1016/j.biopha.2021.111748.

47. The KRAS(G12D) inhibitor MRTX1133 elucidates KRAS-mediated oncogenesis. (2022). Nat Med *28*, 2017-2018. 10.1038/s41591-022-02008-6.

48. Mathews, L.A., Keller, J.M., Goodwin, B.L., Guha, R., Shinn, P., Mull, R., Thomas, C.J., de Kluyver, R.L., Sayers, T.J., and Ferrer, M. (2012). A 1536-well quantitative high-throughput screen to identify compounds targeting cancer stem cells. J Biomol Screen *17*, 1231-1242. 10.1177/1087057112458152.

49. Quinlan, M.P., Quatela, S.E., Philips, M.R., and Settleman, J. (2008). Activated Kras, but not Hras or Nras, may initiate tumors of endodermal origin via stem cell expansion. Mol Cell Biol *28*, 2659-2674. 10.1128/MCB.01661-07.

50. Wang, M.T., Holderfield, M., Galeas, J., Delrosario, R., To, M.D., Balmain, A., and McCormick, F. (2015). K-Ras Promotes Tumorigenicity through Suppression of Non-canonical Wnt Signaling. Cell *163*, 1237-1251. 10.1016/j.cell.2015.10.041.

51. Najumudeen, A.K., Jaiswal, A., Lectez, B., Oetken-Lindholm, C., Guzman, C., Siljamaki, E., Posada, I.M., Lacey, E., Aittokallio, T., and Abankwa, D. (2016). Cancer stem cell drugs target K-ras signaling in a stemness context. Oncogene *35*, 5248-5262. 10.1038/onc.2016.59.

52. Chippalkatti, R., and Abankwa, D. (2021). Promotion of cancer cell stemness by Ras. Biochem Soc Trans *49*, 467-476. 10.1042/BST20200964.

53. Gupta, P.B., Onder, T.T., Jiang, G., Tao, K., Kuperwasser, C., Weinberg, R.A., and Lander, E.S. (2009). Identification of selective inhibitors of cancer stem cells by high-throughput screening. *138*, 645-659. papers3://publication/doi/10.1016/j.cell.2009.06.034.

54. Siddiqui, F.A., Vukic, V., Salminen, T.A., and Abankwa, D. (2021). Elaiophylin Is a Potent Hsp90/Cdc37 Protein Interface Inhibitor with K-Ras Nanocluster Selectivity. Biomolecules *11*. 10.3390/biom11060836.

55. Okutachi, S., Manoharan, G.B., Kiriazis, A., Laurini, C., Catillon, M., McCormick, F., Yli-Kauhaluoma, J., and Abankwa, D. (2021). A Covalent Calmodulin Inhibitor as a Tool to Study Cellular Mechanisms of K-Ras-Driven Stemness. Front Cell Dev Biol *9*, 665673. 10.3389/fcell.2021.665673.

56. Canon, J., Rex, K., Saiki, A.Y., Mohr, C., Cooke, K., Bagal, D., Gaida, K., Holt, T., Knutson, C.G., Koppada, N., et al. (2019). The clinical KRAS(G12C) inhibitor AMG 510 drives anti-tumour immunity. Nature *575*, 217-223. 10.1038/s41586-019-1694-1.

57. Fell, J.B., Fischer, J.P., Baer, B.R., Blake, J.F., Bouhana, K., Briere, D.M., Brown, K.D., Burgess, L.E., Burns, A.C., Burkard, M.R., et al. (2020). Identification of the Clinical Development Candidate MRTX849, a Covalent KRAS(G12C) Inhibitor for the Treatment of Cancer. J Med Chem *63*, 6679-6693. 10.1021/acs.jmedchem.9b02052.

58. Janes, M.R., Zhang, J., Li, L.S., Hansen, R., Peters, U., Guo, X., Chen, Y., Babbar, A., Firdaus, S.J., Darjania, L., et al. (2018). Targeting KRAS Mutant Cancers with a Covalent G12C-Specific Inhibitor. Cell *172*, 578-589 e517. 10.1016/j.cell.2018.01.006.

59. Wang, X., Allen, S., Blake, J.F., Bowcut, V., Briere, D.M., Calinisan, A., Dahlke, J.R., Fell, J.B., Fischer, J.P., Gunn, R.J., et al. (2022). Identification of MRTX1133, a Noncovalent, Potent, and Selective KRAS(G12D) Inhibitor. J Med Chem *65*, 3123-3133. 10.1021/acs.jmedchem.1c01688.

60. Steffen, C.L., Kaya, P., Schaffner-Reckinger, E., and Abankwa, D. (2023). Eliminating oncogenic RAS: back to the future at the drawing board. Biochem Soc Trans. 10.1042/BST20221343.

61. Abankwa, D., Gorfe, A.A., Inder, K., and Hancock, J.F. (2010). Ras membrane orientation and nanodomain localization generate isoform diversity. Proc Natl Acad Sci U S A *107*, 1130-1135. 10.1073/pnas.0903907107.

62. Yelland, T., Garcia, E., Parry, C., Kowalczyk, D., Wojnowska, M., Gohlke, A., Zalar, M., Cameron, K., Goodwin, G., Yu, Q., et al. (2022). Stabilization of the RAS:PDE6D Complex Is a Novel Strategy to Inhibit RAS Signaling. J Med Chem *65*, 1898-1914. 10.1021/acs.jmedchem.1c01265.

63. Cirstea, I.C., Gremer, L., Dvorsky, R., Zhang, S.C., Piekorz, R.P., Zenker, M., and Ahmadian, M.R. (2013). Diverging gain-of-function mechanisms of two novel KRAS mutations associated with Noonan and cardio-facio-cutaneous syndromes. Hum Mol Genet *22*, 262-270. 10.1093/hmg/dds426.

64. Wall, V.E., Garvey, L.A., Mehalko, J.L., Procter, L.V., and Esposito, D. (2014). Combinatorial assembly of clone libraries using site-specific recombination. Methods Mol Biol *1116*, 193-208. 10.1007/978-1-62703-764-8_14.

65. Duggan, M.C., Regan-Fendt, K., Olaverria Salavaggione, G.N., Howard, J.H., Stiff, A.R., Sabella, J., Latchana, N., Markowitz, J., Gru, A., Tridandapani, S., et al. (2019). Neuroblastoma RAS viral oncogene homolog mRNA is differentially spliced to give five distinct isoforms: implications for melanoma therapy. Melanoma Res *29*, 491-500. 10.1097/CMR.0000000000000623.

66. Livak, K.J., and Schmittgen, T.D. (2001). Analysis of relative gene expression data using real-time quantitative PCR and the 2(-Delta Delta C(T)) Method. Methods *25*, 402-408. 10.1006/meth.2001.1262.

67. Xu, Q., and Wu, Z. (2000). The insulin-like growth factor-phosphatidylinositol 3-kinase-Akt signaling pathway regulates myogenin expression in normal myogenic cells but not in rhabdomyosarcoma-derived RD cells. J Biol Chem *275*, 36750-36757. 10.1074/jbc.M005030200.

68. Velica, P., and Bunce, C.M. (2011). A quick, simple and unbiased method to quantify C2C12 myogenic differentiation. Muscle Nerve *44*, 366-370. 10.1002/mus.22056.

69. Goto, H., Tomono, Y., Ajiro, K., Kosako, H., Fujita, M., Sakurai, M., Okawa, K., Iwamatsu, A., Okigaki, T., Takahashi, T., and Inagaki, M. (1999). Identification of a novel phosphorylation site on histone H3 coupled with mitotic chromosome condensation. J Biol Chem *274*, 25543-25549. 10.1074/jbc.274.36.25543.

70. Chia, W., Somers, W.G., and Wang, H. (2008). Drosophila neuroblast asymmetric divisions: cell cycle regulators, asymmetric protein localization, and tumorigenesis. J Cell Biol *180*, 267-272. 10.1083/jcb.200708159.

71. Garcia-Espana, A., and Philips, M.R. (2023). Origin and Evolution of RAS Membrane Targeting. Oncogene *42*, 1741-1750. 10.1038/s41388-023-02672-z.

72. Konieczny, S.F., Drobes, B.L., Menke, S.L., and Taparowsky, E.J. (1989). Inhibition of myogenic differentiation by the H-ras oncogene is associated with the down regulation of the MyoD1 gene. Oncogene *4*, 473-481.

73. Hobbs, G.A., Der, C.J., and Rossman, K.L. (2016). RAS isoforms and mutations in cancer at a glance. J Cell Sci *129*, 1287-1292. 10.1242/jcs.182873.

74. Stevenson, D.A., Allen, S., Tidyman, W.E., Carey, J.C., Viskochil, D.H., Stevens, A., Hanson, H., Sheng, X., Thompson, B.A., Okumura, M.J., et al. (2012). Peripheral muscle weakness in RASopathies. Muscle Nerve *46*, 394-399. 10.1002/mus.23324.

75. Bustelo, X.R., Crespo, P., Fernandez-Pisonero, I., and Rodriguez-Fdez, S. (2018). RAS GTPase-dependent pathways in developmental diseases: old guys, new lads, and current challenges. Curr Opin Cell Biol *55*, 42-51. 10.1016/j.ceb.2018.06.007.

76. Schubbert, S., Zenker, M., Rowe, S.L., Boll, S., Klein, C., Bollag, G., van der Burgt, I., Musante, L., Kalscheuer, V., Wehner, L.E., et al. (2006). Germline KRAS mutations cause Noonan syndrome. Nat Genet *38*, 331-336. 10.1038/ng1748.

77. Punekar, S.R., Velcheti, V., Neel, B.G., and Wong, K.K. (2022). The current state of the art and future trends in RAS-targeted cancer therapies. Nat Rev Clin Oncol *19*, 637-655. 10.1038/s41571-022-00671-9.

78. Hallin, J., Bowcut, V., Calinisan, A., Briere, D.M., Hargis, L., Engstrom, L.D., Laguer, J., Medwid, J., Vanderpool, D., Lifset, E., et al. (2022). Anti-tumor efficacy of a potent and selective non-covalent KRAS^{G12D} inhibitor. Nat Med *28*, 2171-2182. 10.1038/s41591-022-02007-7.

79. Zembruski, N.C., Stache, V., Haefeli, W.E., and Weiss, J. (2012). 7-Aminoactinomycin D for apoptosis staining in flow cytometry. Anal Biochem *429*, 79-81. 10.1016/j.ab.2012.07.005.

80. Lau, H.Y., Ramanujulu, P.M., Guo, D., Yang, T., Wirawan, M., Casey, P.J., Go, M.L., and Wang, M. (2014). An improved isoprenylcysteine carboxylmethyltransferase inhibitor induces cancer cell death and attenuates tumor growth in vivo. Cancer Biol Ther *15*, 1280-1291. 10.4161/cbt.29692.

81. Whyte, D.B., Kirschmeier, P., Hockenberry, T.N., Nunez-Oliva, I., James, L., Catino, J.J., Bishop, W.R., and Pai, J.K. (1997). K- and N-Ras are geranylgeranylated in cells treated with farnesyl protein transferase inhibitors. J Biol Chem *272*, 14459-14464. 10.1074/jbc.272.22.14459.

82. Gebregiworgis, T., Kano, Y., St-Germain, J., Radulovich, N., Udaskin, M.L., Mentes, A., Huang, R., Poon, B.P.K., He, W., Valencia-Sama, I., et al. (2021). The Q61H mutation decouples KRAS from upstream regulation and renders cancer cells resistant to SHP2 inhibitors. Nat Commun *12*, 6274. 10.1038/s41467-021-26526-y.

83. Hofmann, M.H., Gmachl, M., Ramharter, J., Savarese, F., Gerlach, D., Marszalek, J.R., Sanderson, M.P., Kessler, D., Trapani, F., Arnhof, H., et al. (2021). BI-3406, a Potent and Selective SOS1-

KRAS Interaction Inhibitor, Is Effective in KRAS-Driven Cancers through Combined MEK Inhibition. Cancer Discov *11*, 142-157. 10.1158/2159-8290.CD-20-0142.

84. Vasta, J.D., Peacock, D.M., Zheng, Q., Walker, J.A., Zhang, Z., Zimprich, C.A., Thomas, M.R., Beck, M.T., Binkowski, B.F., Corona, C.R., Robers, M.B., and Shokat, K.M. (2022). KRAS is vulnerable to reversible switch-II pocket engagement in cells. Nat Chem Biol *18*, 596-604. 10.1038/s41589-022-00985-w.

85. Ho, A.L., Brana, I., Haddad, R., Bauman, J., Bible, K., Oosting, S., Wong, D.J., Ahn, M.J., Boni, V., Even, C., et al. (2021). Tipifarnib in Head and Neck Squamous Cell Carcinoma With HRAS Mutations. J Clin Oncol *39*, 1856-1864. 10.1200/JCO.20.02903.

86. Skoulidis, F., Li, B.T., Dy, G.K., Price, T.J., Falchook, G.S., Wolf, J., Italiano, A., Schuler, M., Borghaei, H., Barlesi, F., et al. (2021). Sotorasib for Lung Cancers with KRAS p.G12C Mutation. N Engl J Med *384*, 2371-2381. 10.1056/NEJMoa2103695.

87. Esposito, D., Stephen, A.G., Turbyville, T.J., and Holderfield, M. (2019). New weapons to penetrate the armor: Novel reagents and assays developed at the NCI RAS Initiative to enable discovery of RAS therapeutics. Semin Cancer Biol *54*, 174-182. 10.1016/j.semcancer.2018.02.006.

88. Desbordes, S.C., Placantonakis, D.G., Ciro, A., Socci, N.D., Lee, G., Djaballah, H., and Studer, L. (2008). High-throughput screening assay for the identification of compounds regulating self-renewal and differentiation in human embryonic stem cells. Cell Stem Cell *2*, 602-612. 10.1016/j.stem.2008.05.010.

89. Jee, J., Jeon, H., Hwang, D., Sommer, P., Park, Z., Cechetto, J., and Dorval, T. (2012). High content screening for compounds that induce early stages of human embryonic stem cell differentiation. Comb Chem High Throughput Screen *15*, 656-665. 10.2174/138620712802650540.

90. Barbaric, I., Gokhale, P.J., Jones, M., Glen, A., Baker, D., and Andrews, P.W. (2010). Novel regulators of stem cell fates identified by a multivariate phenotype screen of small compounds on human embryonic stem cell colonies. Stem Cell Res *5*, 104-119. 10.1016/j.scr.2010.04.006.

91. Sherman, S.P., and Pyle, A.D. (2013). Small molecule screening with laser cytometry can be used to identify pro-survival molecules in human embryonic stem cells. PLoS One *8*, e54948. 10.1371/journal.pone.0054948.

92. Rommel, C., Clarke, B.A., Zimmermann, S., Nunez, L., Rossman, R., Reid, K., Moelling, K., Yancopoulos, G.D., and Glass, D.J. (1999). Differentiation stage-specific inhibition of the Raf-MEK-ERK pathway by Akt. Science *286*, 1738-1741. 10.1126/science.286.5445.1738.

93. Olson, E.N., Spizz, G., and Tainsky, M.A. (1987). The oncogenic forms of N-ras or H-ras prevent skeletal myoblast differentiation. Mol Cell Biol *7*, 2104-2111. 10.1128/mcb.7.6.2104-2111.1987.

94. Dorman, C.M., and Johnson, S.E. (1999). Activated Raf inhibits avian myogenesis through a MAPK-dependent mechanism. Oncogene *18*, 5167-5176. 10.1038/sj.onc.1202907.

95. Weyman, C.M., and Wolfman, A. (1998). Mitogen-activated protein kinase kinase (MEK) activity is required for inhibition of skeletal muscle differentiation by insulin-like growth factor 1 or fibroblast growth factor 2. Endocrinology *139*, 1794-1800. 10.1210/endo.139.4.5950.

96. Stevenson, D.A., and Yang, F.C. (2011). The musculoskeletal phenotype of the RASopathies. Am J Med Genet C Semin Med Genet *157C*, 90-103. 10.1002/ajmg.c.30296.

97. Tidyman, W.E., Goodwin, A.F., Maeda, Y., Klein, O.D., and Rauen, K.A. (2022). MEK-inhibitor-mediated rescue of skeletal myopathy caused by activating Hras mutation in a Costello syndrome mouse model. Dis Model Mech *15*. 10.1242/dmm.049166.

98. Maeda, Y., Tidyman, W.E., Ander, B.P., Pritchard, C.A., and Rauen, K.A. (2021). Ras/MAPK dysregulation in development causes a skeletal myopathy in an activating Braf(L597V) mouse model for cardio-facio-cutaneous syndrome. Dev Dyn *250*, 1074-1095. 10.1002/dvdy.309.

99. Feige, P., Brun, C.E., Ritso, M., and Rudnicki, M.A. (2018). Orienting Muscle Stem Cells for Regeneration in Homeostasis, Aging, and Disease. Cell Stem Cell *23*, 653-664. 10.1016/j.stem.2018.10.006.

100. Penna, F., Costamagna, D., Fanzani, A., Bonelli, G., Baccino, F.M., and Costelli, P. (2010). Muscle wasting and impaired myogenesis in tumor bearing mice are prevented by ERK inhibition. PLoS One *5*, e13604. 10.1371/journal.pone.0013604.

101. Prado, C.M., Bekaii-Saab, T., Doyle, L.A., Shrestha, S., Ghosh, S., Baracos, V.E., and Sawyer, M.B. (2012). Skeletal muscle anabolism is a side effect of therapy with the MEK inhibitor: selumetinib in patients with cholangiocarcinoma. Br J Cancer *106*, 1583-1586. 10.1038/bjc.2012.144.

102. Skapek, S.X., Ferrari, A., Gupta, A.A., Lupo, P.J., Butler, E., Shipley, J., Barr, F.G., and Hawkins, D.S. (2019). Rhabdomyosarcoma. Nat Rev Dis Primers *5*, 1. 10.1038/s41572-018-0051-2.

103. Shern, J.F., Chen, L., Chmielecki, J., Wei, J.S., Patidar, R., Rosenberg, M., Ambrogio, L., Auclair, D., Wang, J., Song, Y.K., et al. (2014). Comprehensive genomic analysis of rhabdomyosarcoma reveals a landscape of alterations affecting a common genetic axis in fusion-positive and fusion-negative tumors. Cancer Discov *4*, 216-231. 10.1158/2159-8290.CD-13-0639.

104. Yohe, M.E., Gryder, B.E., Shern, J.F., Song, Y.K., Chou, H.C., Sindiri, S., Mendoza, A., Patidar, R., Zhang, X., Guha, R., et al. (2018). MEK inhibition induces MYOG and remodels super-enhancers in RAS-driven rhabdomyosarcoma. Sci Transl Med *10*. 10.1126/scitranslmed.aan4470.

105. Pal, R., Mamidi, M.K., Das, A.K., and Bhonde, R. (2012). Diverse effects of dimethyl sulfoxide (DMSO) on the differentiation potential of human embryonic stem cells. Arch Toxicol *86*, 651-661. 10.1007/s00204-011-0782-2.

106. Chen, T.H., Wang, Y.H., and Wu, Y.H. (2011). Developmental exposures to ethanol or dimethylsulfoxide at low concentrations alter locomotor activity in larval zebrafish: implications for behavioral toxicity bioassays. Aquat Toxicol *102*, 162-166. 10.1016/j.aquatox.2011.01.010.

107. Hatfield, I., Harvey, I., Yates, E.R., Redd, J.R., Reiter, L.T., and Bridges, D. (2015). The role of TORC1 in muscle development in Drosophila. Sci Rep *5*, 9676. 10.1038/srep09676.

108. Mounier, R., Lantier, L., Leclerc, J., Sotiropoulos, A., Foretz, M., and Viollet, B. (2011). Antagonistic control of muscle cell size by AMPK and mTORC1. Cell Cycle *10*, 2640-2646. 10.4161/cc.10.16.17102.

109. Yoon, M.S. (2017). mTOR as a Key Regulator in Maintaining Skeletal Muscle Mass. Front Physiol *8*, 788. 10.3389/fphys.2017.00788.

110. Joseph, G.A., Wang, S.X., Jacobs, C.E., Zhou, W., Kimble, G.C., Tse, H.W., Eash, J.K., Shavlakadze, T., and Glass, D.J. (2019). Partial Inhibition of mTORC1 in Aged Rats Counteracts the Decline in Muscle Mass and Reverses Molecular Signaling Associated with Sarcopenia. Mol Cell Biol *39*. 10.1128/MCB.00141-19.

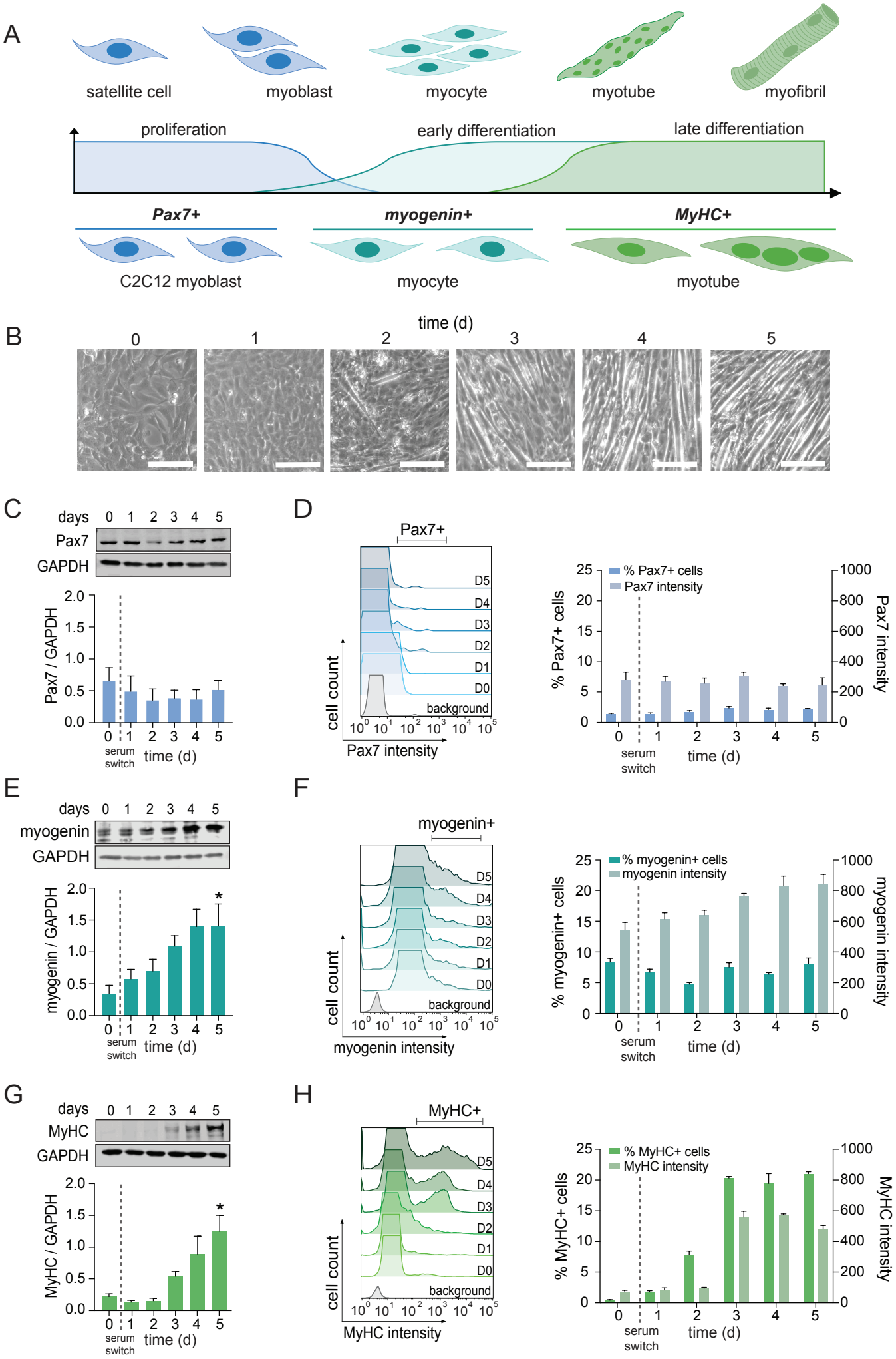
A
satellite cell
myoblast
myocyte
myotube
myofibril
proliferation
early differentiation
late differentiation
Pax7+
myogenin+
MyHC+
C2C12 myoblast
myocyte
myotube
B
time (d)
0
1
2
3
4
5
C
days 0 1 2 3 4 5
Pax7
GAPDH
Pax7 / GAPDH
serum switch
time (d)
D
Pax7+
D5
D4
D3
D2
D1
D0
background
cell count
Pax7 intensity
% Pax7+ cells
Pax7 intensity
E
days 0 1 2 3 4 5
myogenin
GAPDH
myogenin / GAPDH
F
myogenin+
myogenin intensity
% myogenin+ cells
myogenin intensity
G
days 0 1 2 3 4 5
MyHC
GAPDH
MyHC / GAPDH
H
MyHC+
MyHC intensity
% MyHC+ cells
MyHC intensity

Figure 1

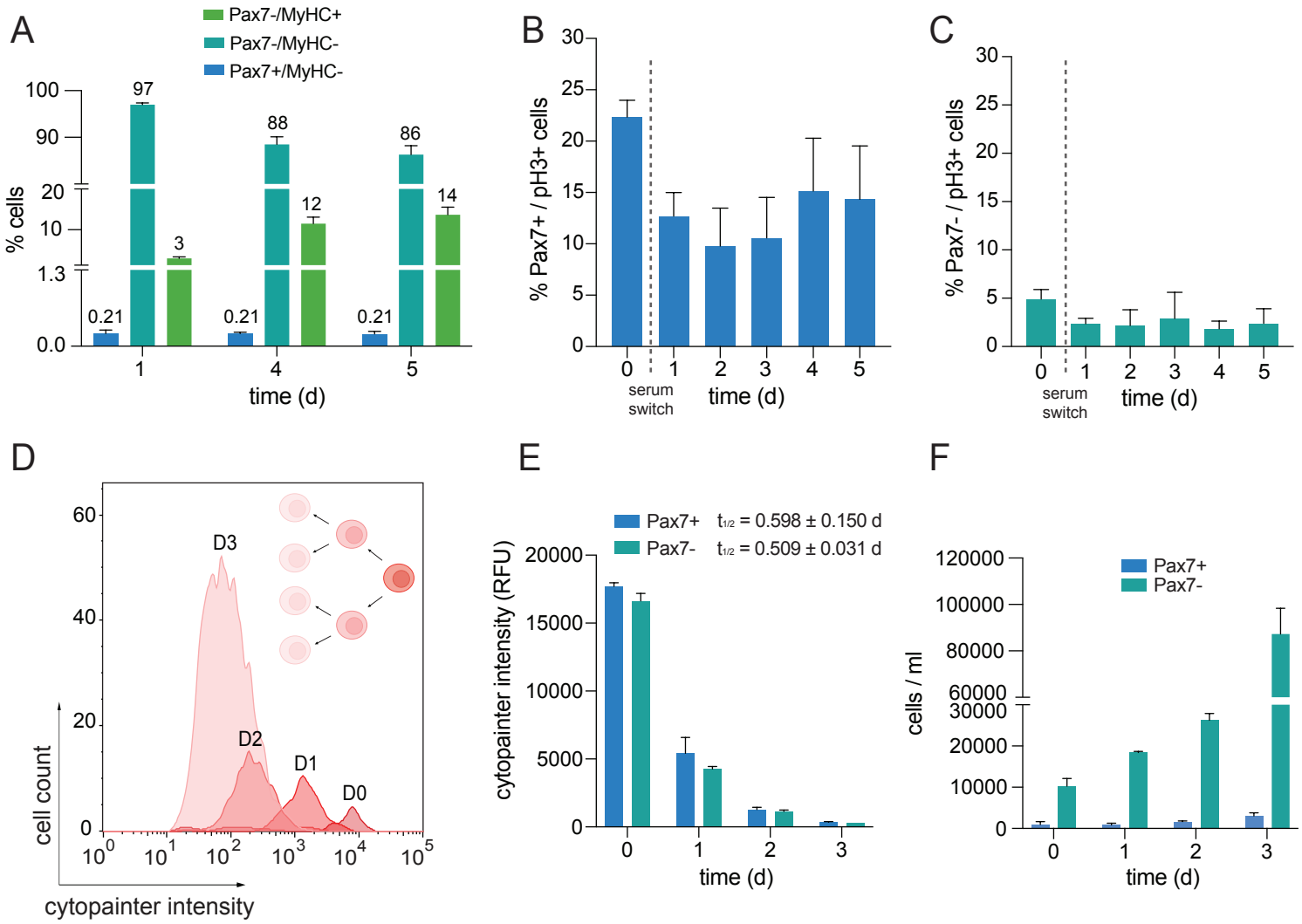
A
Pax7-/MyHC+
Pax7-/MyHC-
Pax7+/MyHC-
% cells
time (d)
B
% Pax7+ / pH3+ cells
serum switch
time (d)
C
% Pax7- / pH3+ cells
serum switch
time (d)
D
cell count
cytopainter intensity
D3
D2
D1
D0
E
Pax7+ t1/2 = 0.598 ± 0.150 d
Pax7- t1/2 = 0.509 ± 0.031 d
cytopainter intensity (RFU)
time (d)
F
Pax7+
Pax7-
cells / ml
time (d)

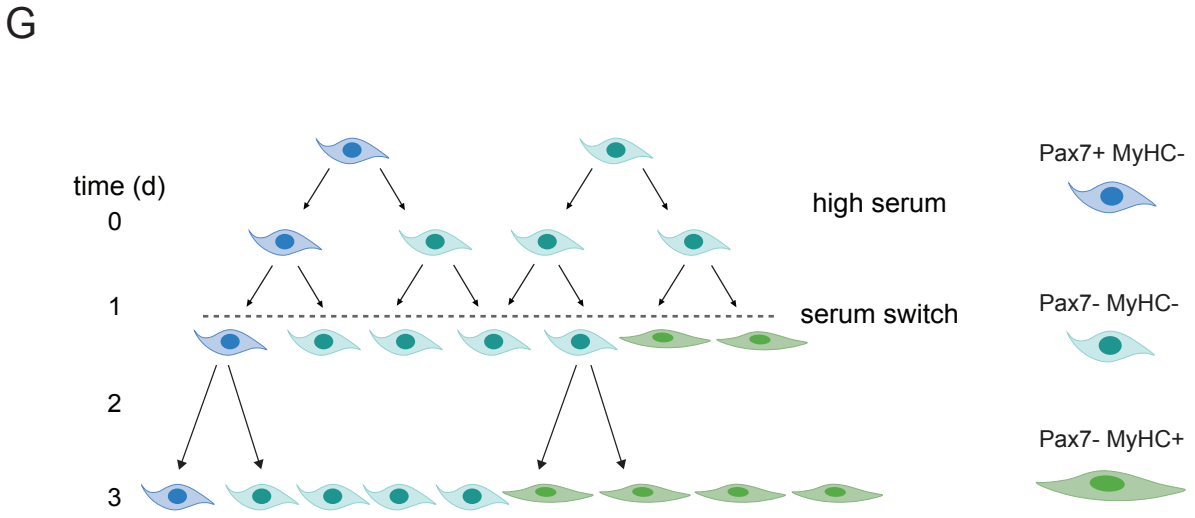
G
time (d)
high serum
serum switch
Pax7+ MyHC-
Pax7- MyHC-
Pax7- MyHC+

Figure 2

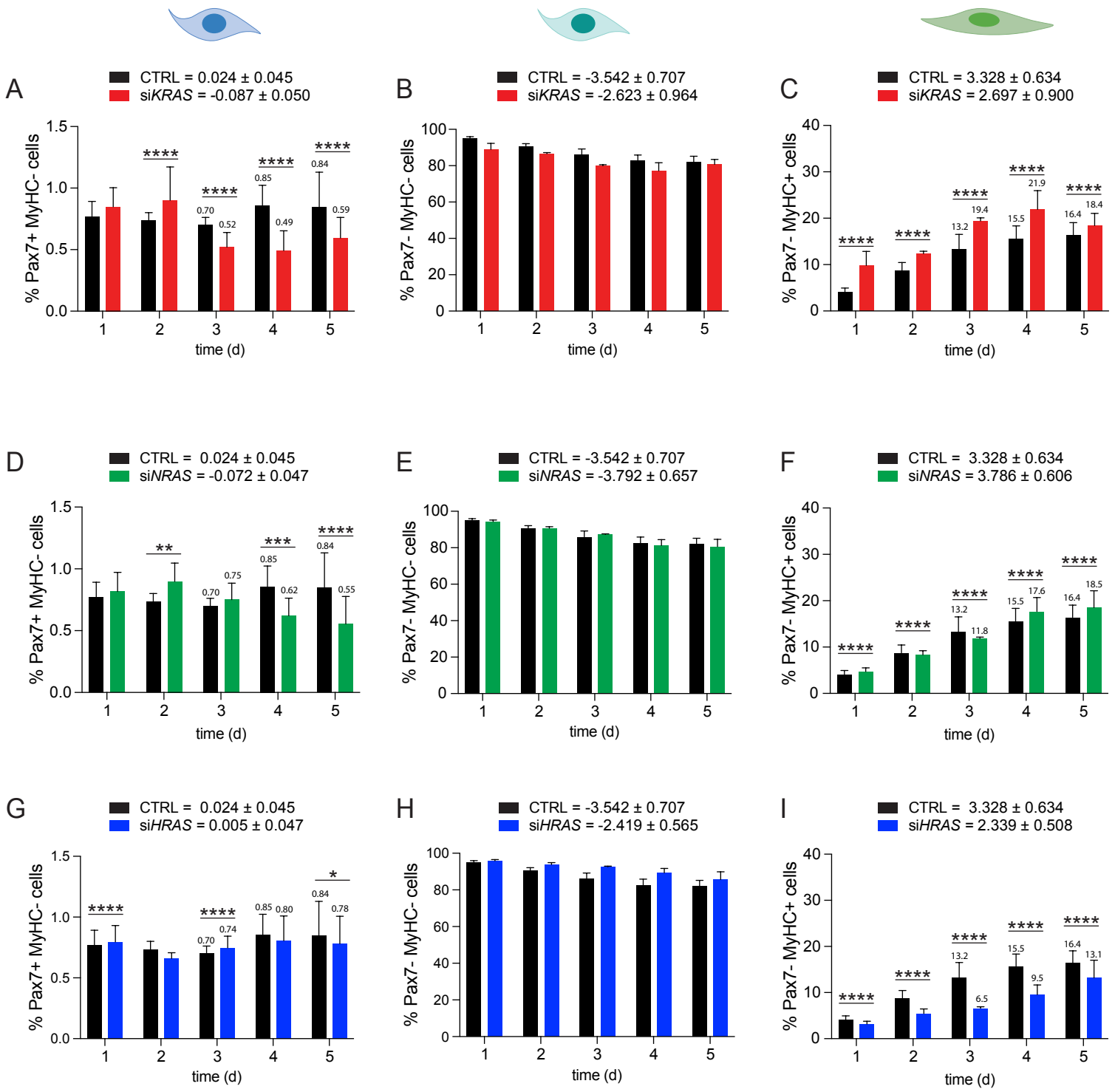
A
CTRL = 0.024 ± 0.045
siKRAS = -0.087 ± 0.050
% Pax7+ MyHC- cells
time (d)
B
CTRL = -3.542 ± 0.707
siKRAS = -2.623 ± 0.964
% Pax7- MyHC- cells
time (d)
C
CTRL = 3.328 ± 0.634
siKRAS = 2.697 ± 0.900
% Pax7- MyHC+ cells
time (d)
D
CTRL = 0.024 ± 0.045
siNRAS = -0.072 ± 0.047
% Pax7+ MyHC- cells
time (d)
E
CTRL = -3.542 ± 0.707
siNRAS = -3.792 ± 0.657
% Pax7- MyHC- cells
time (d)
F
CTRL = 3.328 ± 0.634
siNRAS = 3.786 ± 0.606
% Pax7- MyHC+ cells
time (d)
G
CTRL = 0.024 ± 0.045
siHRAS = 0.005 ± 0.047
% Pax7+ MyHC- cells
time (d)
H
CTRL = -3.542 ± 0.707
siHRAS = -2.419 ± 0.565
% Pax7- MyHC- cells
time (d)
I
CTRL = 3.328 ± 0.634
siHRAS = 2.339 ± 0.508
% Pax7- MyHC+ cells
time (d)

Figure 3

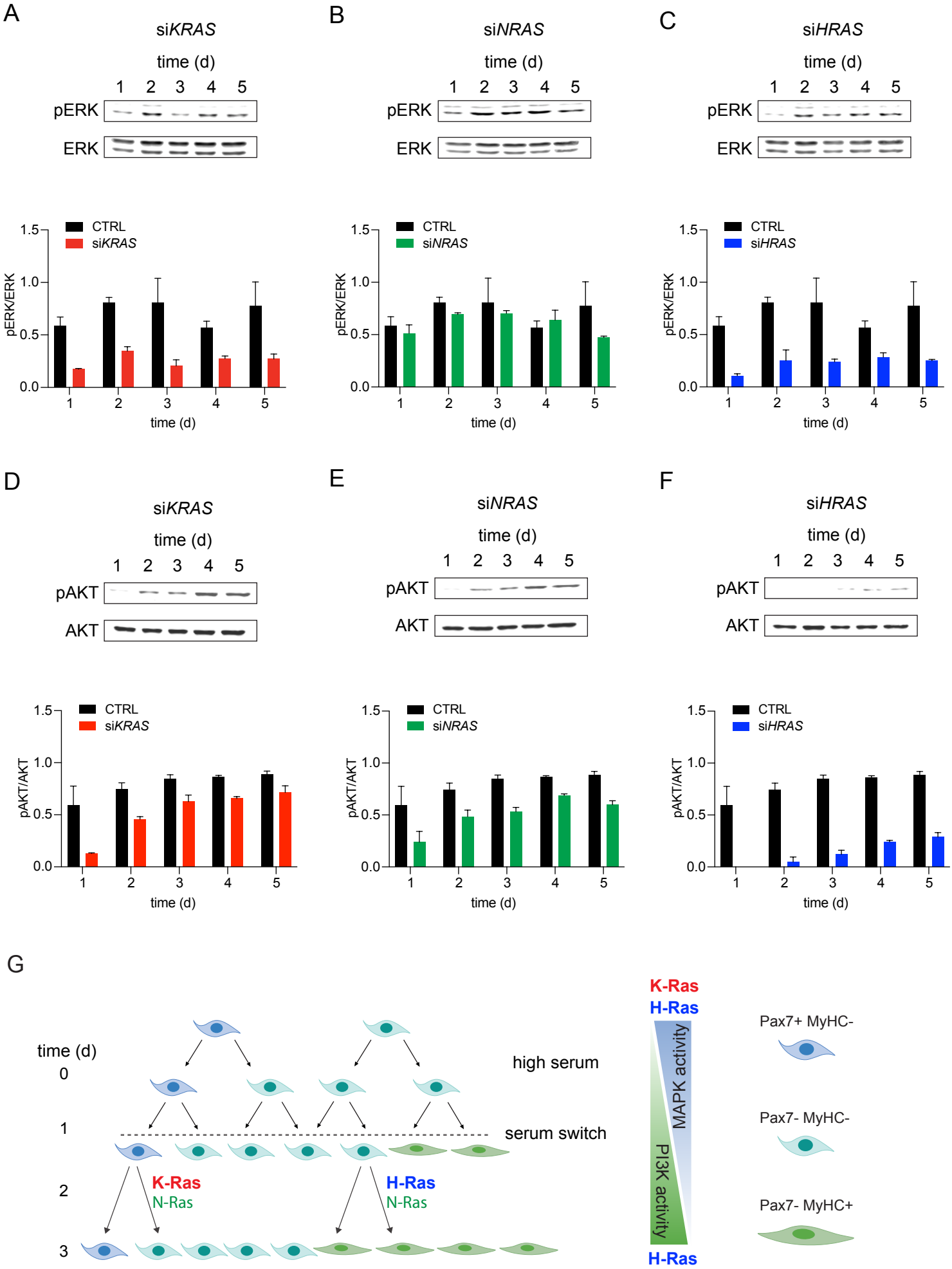
A
siKRAS
time (d)
1 2 3 4 5
pERK
ERK
B
siNRAS
C
siHRAS
CTRL
siKRAS
siNRAS
siHRAS
pERK/ERK
time (d)
D
E
F
pAKT
AKT
pAKT/AKT
G
time (d)
0
1
2
3
high serum
serum switch
K-Ras
N-Ras
H-Ras
MAPK activity
PI3K activity
Pax7+ MyHC-
Pax7- MyHC-
Pax7- MyHC+

Figure 4

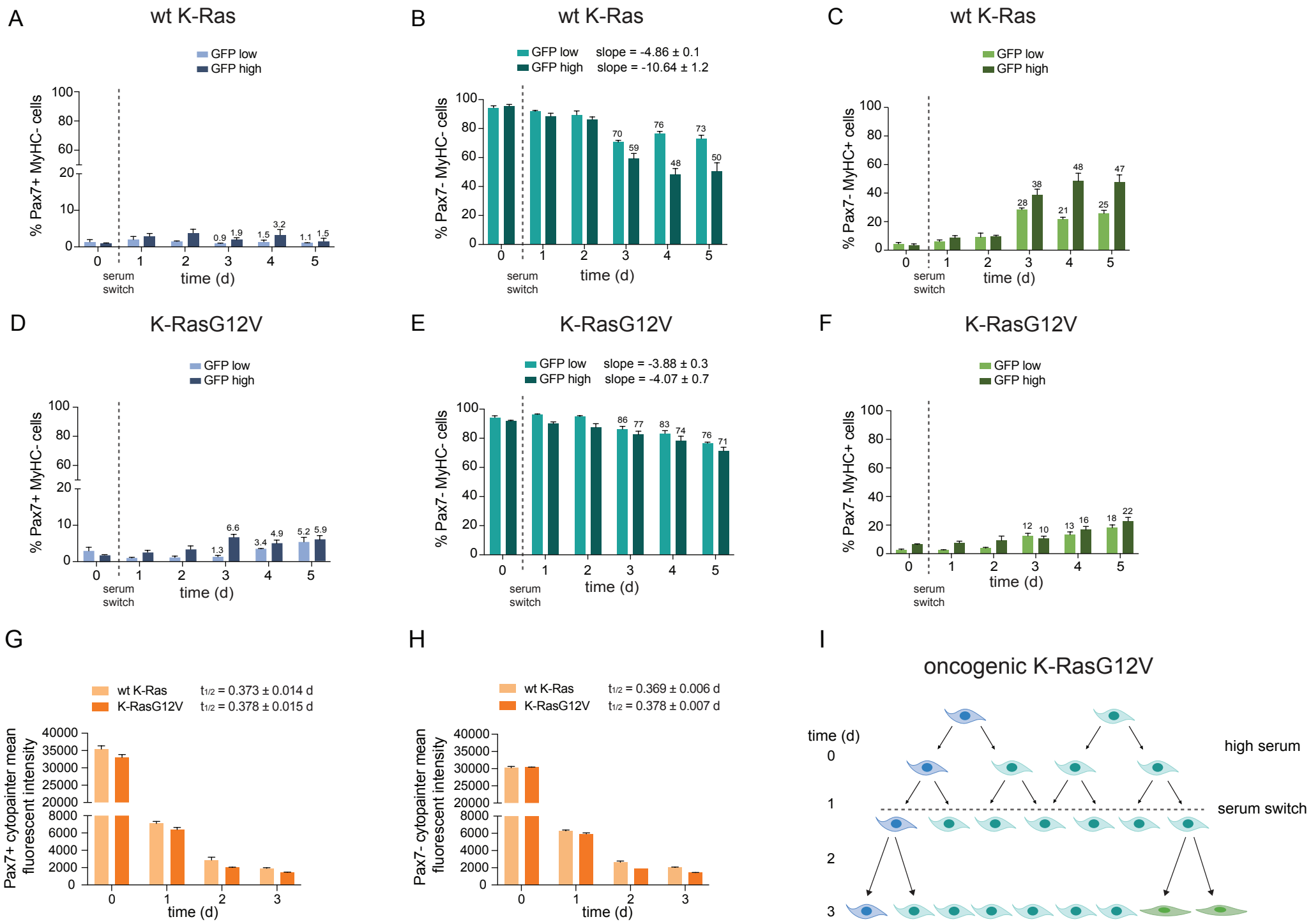
A
wt K-Ras
GFP low
GFP high
% Pax7+ MyHC- cells
100
80
60
20
10
0
0.9
1.9
1.5
3.2
1.1
1.5
0
1
2
3
4
5
serum switch
time (d)
B
wt K-Ras
GFP low slope = -4.86 ± 0.1
GFP high slope = -10.64 ± 1.2
% Pax7- MyHC- cells
100
80
60
40
20
0
70
59
76
48
73
50
0
1
2
3
4
5
serum switch
time (d)
C
wt K-Ras
GFP low
GFP high
% Pax7- MyHC+ cells
100
80
60
40
20
0
28
38
21
48
25
47
0
1
2
3
4
5
serum switch
time (d)
D
K-RasG12V
GFP low
GFP high
% Pax7+ MyHC- cells
100
80
60
20
10
0
1.3
6.6
3.4
4.9
5.2
5.9
0
1
2
3
4
5
serum switch
time (d)
E
K-RasG12V
GFP low slope = -3.88 ± 0.3
GFP high slope = -4.07 ± 0.7
% Pax7- MyHC- cells
100
80
60
40
20
0
86
77
83
74
76
71
0
1
2
3
4
5
serum switch
time (d)
F
K-RasG12V
GFP low
GFP high
% Pax7- MyHC+ cells
100
80
60
40
20
0
12
10
13
16
18
22
0
1
2
3
4
5
serum switch
time (d)
G
wt K-Ras $t_{1/2}$ = 0.373 ± 0.014 d
K-RasG12V $t_{1/2}$ = 0.378 ± 0.015 d
Pax7+ cytopainter mean fluorescent intensity
40000
35000
30000
25000
20000
8000
6000
4000
2000
0
0
1
2
3
time (d)
H
wt K-Ras $t_{1/2}$ = 0.369 ± 0.006 d
K-RasG12V $t_{1/2}$ = 0.378 ± 0.007 d
Pax7- cytopainter mean fluorescent intensity
40000
35000
30000
25000
20000
8000
6000
4000
2000
0
0
1
2
3
time (d)
I
oncogenic K-RasG12V
time (d)
0
1
2
3
high serum
serum switch

Figure 5

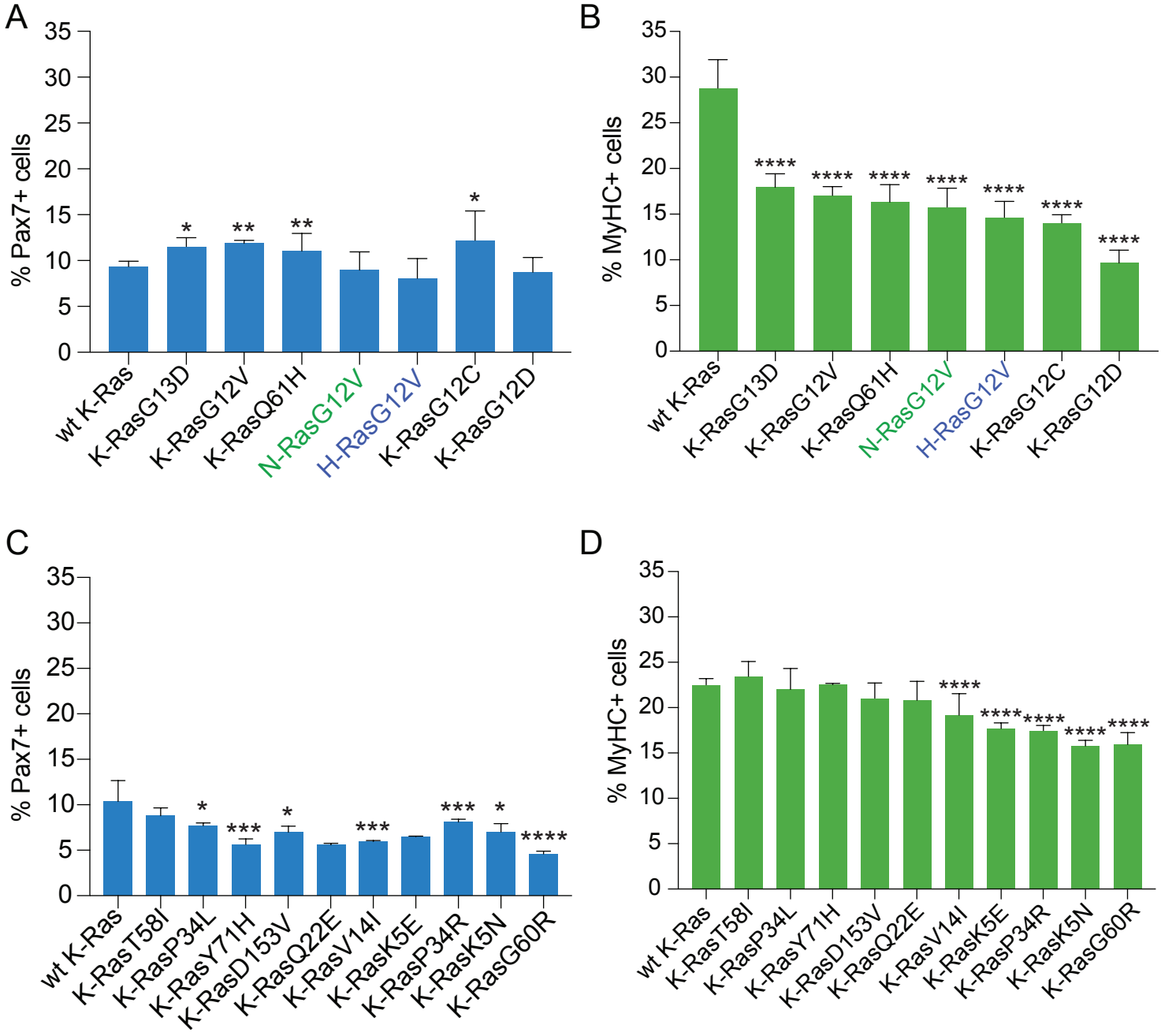
A
% Pax7+ cells
35
30
25
20
15
10
5
0
*
**
**
*
wt K-Ras
K-RasG13D
K-RasG12V
K-RasQ61H
N-RasG12V
H-RasG12V
K-RasG12C
K-RasG12D
B
% MyHC+ cells
****
C
% Pax7+ cells
***
K-RasT58I
K-RasP34L
K-RasY71H
K-RasD153V
K-RasQ22E
K-RasV14I
K-RasK5E
K-RasP34R
K-RasK5N
K-RasG60R
D
% MyHC+ cells

Figure 6

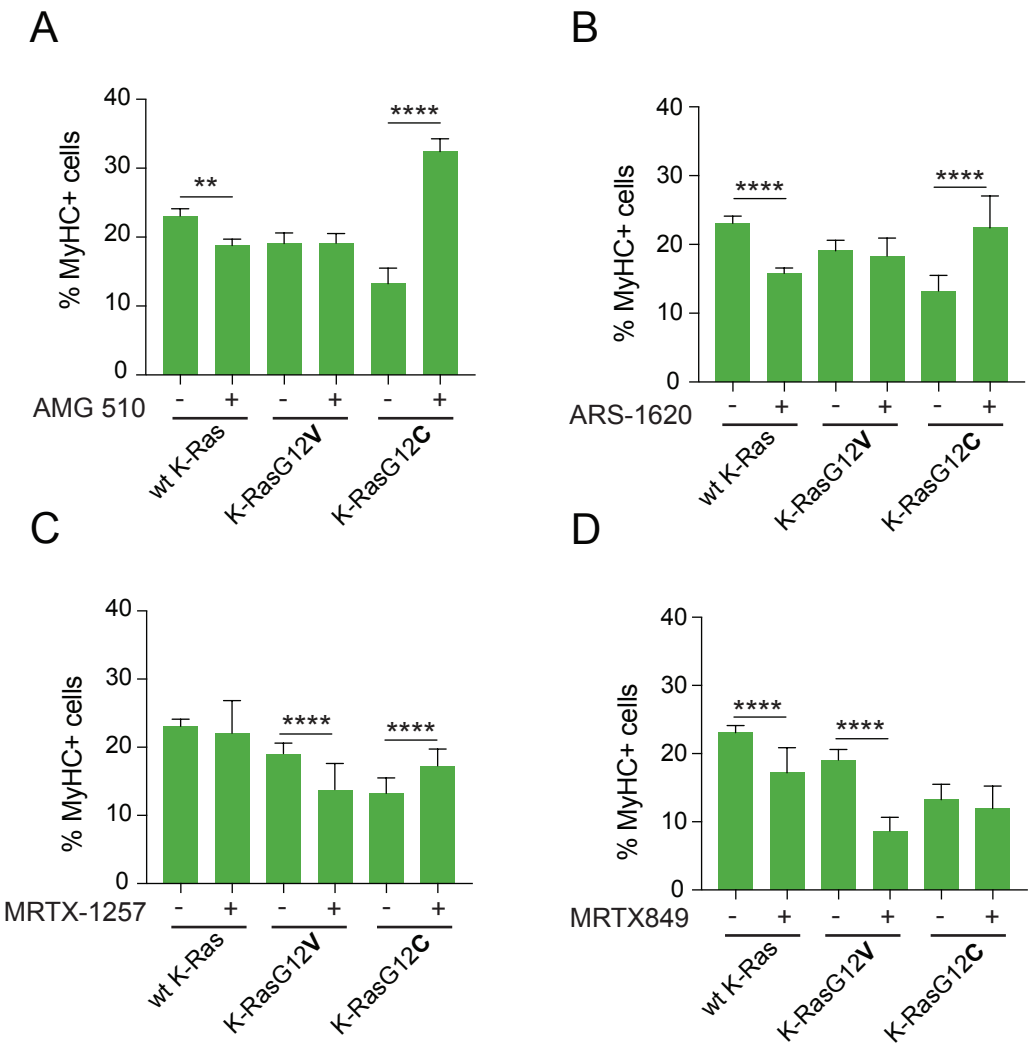
A
% MyHC+ cells
40
30
20
10
0
**
****
AMG 510
-
+
-
+
-
+
wt K-Ras
K-RasG12V
K-RasG12C
B
% MyHC+ cells
40
30
20
10
0
****
****
ARS-1620
-
+
-
+
-
+
wt K-Ras
K-RasG12V
K-RasG12C
C
% MyHC+ cells
40
30
20
10
0
****
****
MRTX-1257
-
+
-
+
-
+
wt K-Ras
K-RasG12V
K-RasG12C
D
% MyHC+ cells
40
30
20
10
0
****
****
MRTX849
-
+
-
+
-
+
wt K-Ras
K-RasG12V
K-RasG12C

Figure 7

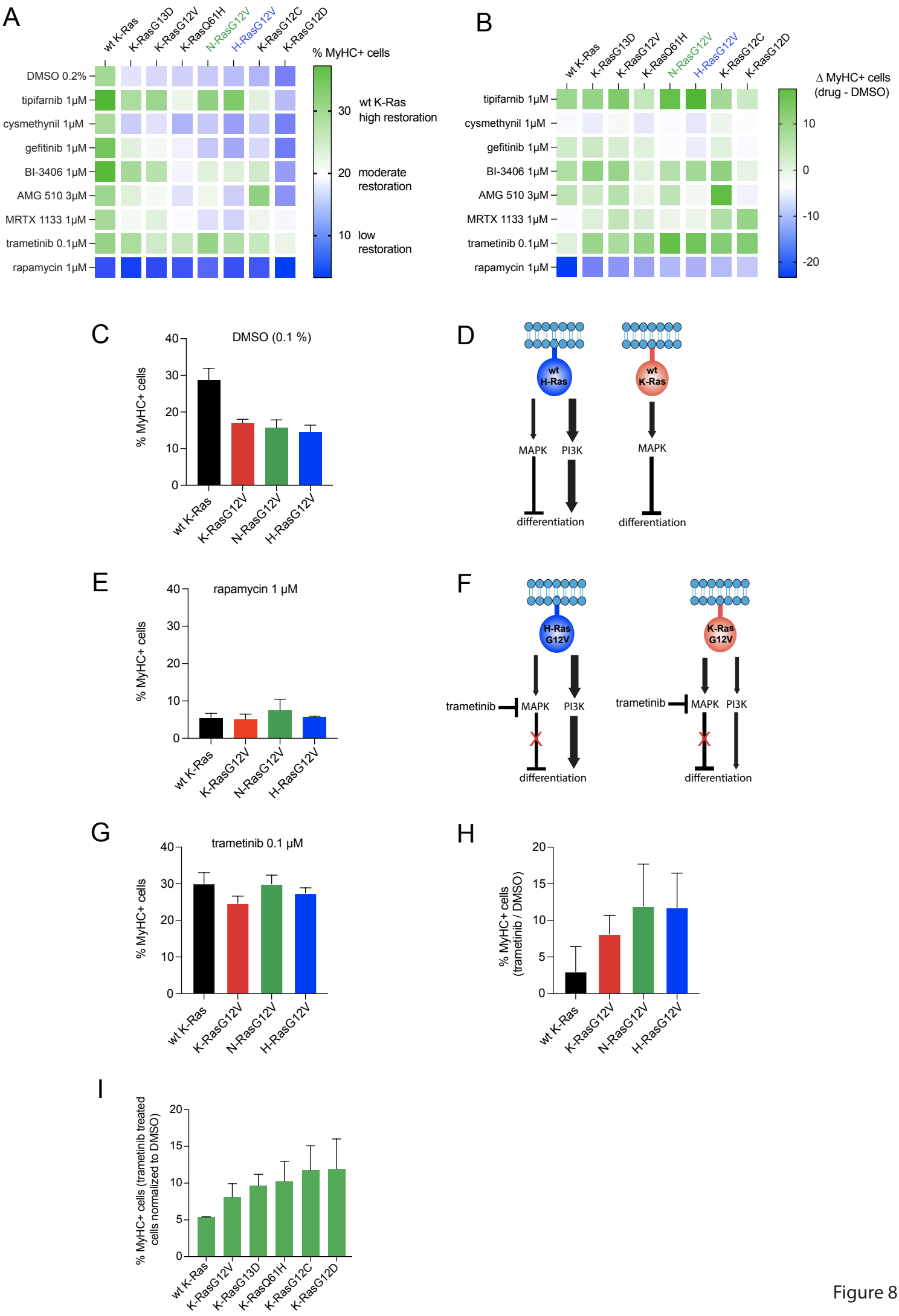
A
wt K-Ras
K-RasG13D
K-RasG12V
K-RasQ61H
N-RasG12V
H-RasG12V
K-RasG12C
K-RasG12D
% MyHC+ cells
DMSO 0.2%
tipifarnib 1μM
cysmethynil 1μM
gefitinib 1μM
BI-3406 1μM
AMG 510 3μM
MRTX 1133 1μM
trametinib 0.1μM
rapamycin 1μM
30 wt K-Ras high restoration
20 moderate restoration
10 low restoration
B
Δ MyHC+ cells (drug - DMSO)
10
0
-10
-20
C
DMSO (0.1 %)
% MyHC+ cells
D
wt H-Ras
wt K-Ras
MAPK
PI3K
differentiation
E
rapamycin 1 μM
F
H-Ras G12V
K-Ras G12V
trametinib
G
trametinib 0.1 μM
H
% MyHC+ cells (trametinib / DMSO)
I
% MyHC+ cells (trametinib treated cells normalized to DMSO)

Figure 8